Available online at www.sciencedirect.com
ScienceDirect
Geochimica et Cosmochimica Acta 71 (2007) 877–894
Geochimica
www.elsevier.com/locate/gca

Transformations of mercury, iron, and sulfur during the reductive dissolution of iron oxyhydroxide by sulfide

Aaron J. Slowey [a,*], Gordon E. Brown Jr. [a,b]

[a] Department of Geological and Environmental Sciences, Stanford University, Stanford, CA 94305-2115, USA
[b] Stanford Synchrotron Radiation Laboratory, SLAC, MS 69, Menlo Park, CA 94025, USA

Received 2 June 2006; accepted in revised form 3 November 2006

Abstract

Methylmercury can accumulate in fish to concentrations unhealthy for humans and other predatory mammals. Most sources of mercury (Hg) emit inorganic species to the environment. Therefore, ecological harm occurs when inorganic Hg is converted to methylmercury. Sulfate- and iron-reducing bacteria (SRB and FeRB) methylate Hg, but the effects of processes involving oxidized and reduced forms of sulfur and iron on the reactivity of Hg, including the propensity of inorganic Hg to be methylated, are poorly understood. Under abiotic conditions, using a laboratory flow reactor, bisulfide (HS^-) was added at 40 to 250 μM h^{-1} to 5 g L^{-1} goethite (α-FeOOH) suspensions to which Hg(II) was adsorbed (30–100 nmol m^{-2}) at pH 7.5. Dissolved Hg initially decreased from 10^3 or 10^4 nM (depending on initial conditions) to 10^{-1} nM, during which the concentration of Hg(II) adsorbed to goethite decreased by 80% and metacinnabar (β-$HgS_{(s)}$) formed, based on identification using Hg L_{III}-edge extended X-ray absorption fine structure (EXAFS) spectroscopic analysis. The apparent coordination of oxygens surrounding Hg(II), measured with EXAFS spectroscopy, increased during one flow experiment, suggesting desorption of monodentate-bound Hg(II) while bidentate-bound Hg(II) persisted on the goethite surface. Further sulfidation increased dissolved Hg concentrations by one to two orders of magnitude (0.5 to 10 nM or 30 nM), suggesting that byproducts of bisulfide oxidation and Fe(III) reduction, primarily polysulfide and potentially Fe(II), enhanced the dissolution of β-$HgS_{(s)}$ and/or desorption of Hg(II). Rapid accumulation of Fe(II) in the solid phase (up to 40 μmol g^{-1}) coincided with faster elevation of dissolved Hg concentrations. Fe(II) served as a proxy for elemental sulfur [S(0)], as S(0) was the dominant bisulfide oxidation product coupled to Fe(III) reduction, based on sulfur K-edge X-ray absorption near edge structure (XANES) spectroscopy. In one experiment, dissolved Hg concentrations tracked those of all sulfide species [S(-II)]. These results suggest that S(-II) reacted with S(0) to form polysulfide, which then caused the dissolution of β-$HgS_{(s)}$. A secondary Fe-bearing phase resembling poorly formed green rust was observed in sulfidized solids with scanning electron microscopy, although there was no clear evidence that either surface-bound or mineralized Fe(II) strongly affected Hg speciation. Examination of interrelated processes involving S(-II) and Fe(III) revealed new modes of Hg solubilization previously not considered in Hg reactivity models.
© 2006 Elsevier Inc. All rights reserved.

1. Introduction

1.1. Background

Innumerable studies of the occurrence and (often operationally defined) speciation of mercury (Hg) indicate that it is a global pollutant of significant importance to the health of fish and predatory mammals, including humans (National Research Council, 2000). While policy decisions in the U.S. have been based, in part, on our current understanding of the behavior of Hg in the environment (U.S. Environmental Protection Agency, 1997), ongoing commitments to monitor Hg in nature suggest a significant degree of uncertainty regarding the extent to which Hg adversely affects ecosystems. For many scientists, the primary objective of monitoring Hg in nature is to test models that estimate methylmercury concentrations in fish based on Hg

* Corresponding author. Present address: U.S. Geological Survey, 345 Middlefield Road, MS 901, Menlo Park, CA 94025, USA. Fax: +1 650 329 5299.
E-mail address: aaron.slowey@gmail.com (A.J. Slowey).

0016-7037/$ - see front matter © 2006 Elsevier Inc. All rights reserved.
doi:10.1016/j.gca.2006.11.011

concentrations in and characteristics of water (Mason et al., 2005; Sveinsdottir and Mason, 2005). These characteristics include wetland area, vegetation, and general physicochemical parameters such as concentrations of suspended solids, organic matter, nutrients, and biological electron acceptors (e.g., nitrate and sulfate) (Bale, 2000; Benoit et al., 2003; Hunter et al., 2003; Barkay and Wagner-Dobler, 2005; Sveinsdottir and Mason, 2005). These models often, however, exclude indicators of biological activity specifically linked to Hg methylation. Sulfate-reducing bacteria (SRB) have long been recognized as important Hg methylators (Compeau and Bartha, 1985; Gilmour et al., 1992; King et al., 2000), and recent studies have confirmed the ability of Fe(III)-reducing bacteria (FeRB) to methylate Hg (Fleming et al., 2006; Kerin et al., in press). Accordingly, sulfide [S(-II)] and ferrous iron [Fe(II)] should be useful indicators of biological activity associated with Hg methylation.

In addition to bacterial activity, a robust model predicting Hg methylation should account for aqueous constituents that affect the reactivity of Hg, specifically its propensity to be methylated. As discussed below, the influence of sulfide on SRB activity and Hg reactivity has been explicitly modeled, but the influence of iron has not. The objective of this study is to investigate how processes cooperatively involving sulfur and iron affect the reactivity of Hg by elucidating and constraining the interactive roles of these constituents under abiotic conditions which were chosen to simulate the chemical effects of the activity of SRB and FeRB.

This study investigates, from an abiotic geochemical perspective, how redox-sensitive interactions between iron and sulfur affect the speciation, and therefore reactivity, of Hg. Using controlled laboratory flow reactors, transformations of Hg, iron, and sulfur were macroscopically and spectroscopically monitored *ex situ* (i.e., in samples extracted from reactors) during the progressive sulfidation of Hg(II) adsorbed to goethite (α-FeOOH).

1.2. Mercury reaction mechanisms in aqueous systems

1.2.1. Mercury speciation and transport

In nearly all Hg-contaminated natural systems, strong particle association has been identified as the primary mode of transport to aquatic environments, whether from mercury mines (Whyte and Kirchner, 2000; Conaway et al., 2003; Lowry et al., 2004; Kim et al., 2004c; Slowey et al., 2005a), alluvial gold mine tailings (Slowey et al., 2005b), or industry (Gagnon et al., 1997; Rolfhus et al., 2003; Bloom et al., 2004). Although particles account for a minor fraction of Hg deposited from the atmosphere to aquatic settings (Ryaboshapko et al., 2002; Poissant et al., 2004; Sakata and Marumoto, 2005), Hg sorption onto particles enhances downward transport to methylating zones in the water column or sediments (Lamborg et al., 2002). While Hg transported from Hg mine tailings is likely dominated by $HgS_{(s)}$ colloids (Lowry et al., 2004; Kim et al., 2004c; Slowey et al., 2005a), the extent of Hg transport through diffusely contaminated fluvial systems has been found to positively co-vary with that of colloidal organic matter (Le Roux et al., 2001); i.e., dissolved Hg strongly partitions to organic or organic-coated inorganic particles. However, once in an estuary or other terminus, microbial oxidation of organic matter may release Hg, which then can resorb to mineral particles (Gagnon et al., 1997). In the Gironde and Seine estuaries (France), sediments enriched in Fe(III)-(hydr)oxides and subject to anaerobiosis were found to be also enriched in Hg (Tseng et al., 2001; Laurier et al., 2003). Thus, the reactivity of Hg sorbed to Fe(III)-(hydr)oxides under anaerobic conditions will likely affect the reactivity of a significant portion of Hg in nature.

1.2.2. Relevant timescales of mercury reactivity

Upon arriving at a contaminated system, changes in Hg speciation on hour-long or shorter timescales likely determine whether it will be rapidly methylated (Moye et al., 2002; Wang and Wong, 2003; Tsui and Wang, 2004). Transport pathways through aquatic systems often involve aerobic to anaerobic transitions (e.g., riparian sedimentation during fluvial transport and deposition in wetland, estuarine, and marine sediments). Transformations of particle-associated Hg during these transitions are little understood, especially on hour-long or shorter timescales. High methylation rates (Eckley et al., 2005) and methylmercury concentrations (Regnell et al., 1997, 2001) have been observed in anoxic hypolimnia, sometimes coinciding with high sulfate reduction rates (Watras et al., 1995). Such findings suggest that changes in Hg speciation at sulfur-bearing redox boundaries can, under some conditions, enhance the propensity for Hg to be methylated on short timescales. Over longer timescales, a fraction of Hg in sediments transforms into presumably less reactive species such as $HgS_{(s)}$ or as a trace substituent in authigenic iron-sulfides (Huerta-Diaz and Morse, 1992; Behra et al., 2001; Wolfenden et al., 2005). Sulfur and iron cycling at redox boundaries in the water column and in sediments, and interactions therewith, strongly affect the reactivity of Hg, including its propensity to be methylated and participate in other *bioavailability processes* (Water Science and Technology Board, 2003) (to be hereafter referred to as *reactivity*).

1.2.3. The effects of sulfur and iron cycling on mercury reactivity

Bacterial sulfur and iron cycles likely control the reactivity of inorganic Hg by changing its speciation. The influence of bacterial sulfate reduction on Hg reactivity is important given that some SRB methylate Hg (Compeau and Bartha, 1985; Gilmour et al., 1992; King et al., 2000; King et al., 2001). Model laboratory studies have demonstrated changes in biologically mediated Hg reactivity due to the precipitation and dissolution of $HgS_{(s)}$ in SRB-containing systems (Benoit et al., 2001a,b; Jay et al., 2002), consistent with an extensive record of S(-II)-Hg reactivity (Hepler and Olofsson, 1975; Clever et al., 1985; Paquette

and Helz, 1997; Tossell, 1999; Jay et al., 2000; Brandon et al., 2001; Tossell, 2001; Charnock et al., 2003; Lennie et al., 2003). The extent to which Hg is methylated in natural systems has been linked to how SRB limit their own activity due to S(-II) toxicity, the extent to which Hg reactivity is controlled by precipitation and dissolution of $HgS_{(s)}$, and the availability of dissolved aqueous Hg species to methylating bacteria (Gilmour et al., 1992; Gilmour et al., 1998; Benoit et al., 1999; Benoit et al., 2003). However, the role of iron in these systems has not been directly studied. Laboratory amendments of natural wetland sediments indicate that Fe(II) potentially affects Hg methylation via interaction with S(-II) (Mehrotra et al., 2003; Mehrotra and Sedlak, 2005). Mechanisms of this interaction and the extent to which it influences Hg reactivity in nature are currently hypothetical. The occurrence and reactivity of S(-II) and iron in natural aquatic systems suggest several conceivable mechanisms by which their interactions may control the reactivity of Hg.

In natural aquatic environments, iron and sulfur often coexist and are reactive to the extent that the concentration of dissolved S(-II) is often limited due to oxidation by Fe(III)-(hydr)oxides (Pyzik and Sommer, 1981; Canfield et al., 1992, 1993; Huerta-Diaz and Morse, 1992; Luther and Church, 1992; Thamdrup et al., 1994; Luther et al., 2003). Where abundant, Fe(III)-(hydr)oxides will therefore mitigate S(-II) toxicity to SRB. While this mitigation may prolong sulfate reduction and therefore indirectly enhance Hg methylation, secondary iron- and sulfur-bearing species may also affect Hg reactivity. Studies of the interaction of Hg with Fe(III)-(hydr)oxide minerals and the latter with sulfide provide the basis for developing hypotheses regarding the combined effects of iron and sulfur-driven processes on Hg speciation. Interestingly, these processes conceivably can decrease or increase Hg reactivity.

While Hg(II) adsorbs to a significant degree to Fe(III)-(hydr)oxide minerals (Barrow and Cox, 1992; Tiffreau et al., 1995), S(-II) in natural systems will likely change the speciation of adsorbed Hg. Under simplified conditions in model aqueous systems, inorganic Hg(II) adsorption readily follows the pH-driven formation of $Hg(OH)_2$ aqueous complexes, while other aqueous ligands such as chloride compete with the adsorbent for Hg(II) (Barrow and Cox, 1992; Gunneriusson and Sjoberg, 1993; Kim et al., 2004a). At the neutral to basic pH common to sulfate-reducing systems (Stumm and Morgan, 1996), bisulfide (HS^-) rapidly binds to the surface of Fe(III)-(hydr)oxide minerals by exchanging with surface hydroxyl groups (dos Santos Afonso and Stumm, 1992). Bisulfide coordination at the Fe(III) (hydr)oxide surface might displace Hg(II) by exchanging for the surface-oriented hydroxyl group:

$$\equiv\mathrm{FeOH}\mathbf{Hg}\mathrm{OH} + \mathrm{HS}^- \rightarrow \equiv\mathrm{FeSH}^- + \mathrm{Hg(OH)_2} \quad (1)$$

Bisulfide may also desorb Hg(II) by complexing it and weakening the surface bond:

$$[\equiv\mathrm{FeOH}\mathbf{Hg}\mathrm{OH} + \mathrm{HS}^- \rightarrow \equiv\mathrm{FeOH}\mathbf{Hg}\mathrm{SH} + \mathrm{OH}^- \rightarrow \equiv\mathrm{FeOH} + \mathrm{Hg(SH)(OH)_{(aq)}} \quad (2)$$

Given a high enough concentration of dissolved Hg(II), excess S(-II) would readily precipitate metacinnabar (β-$HgS_{(s)}$) (Charnock et al., 2003), a thermodynamically unstable form of $HgS_{(s)}$ found to persist in soils (Barnett et al., 1995) and sediments (Kim et al., 2004c; Wolfenden et al., 2005). While β-$HgS_{(s)}$ is often present in soils and sediments, its stability is poorly understood.

$HgS_{(s)}$ is assumed to be relatively stable in the environment, prone to ligand-promoted dissolution by sulfide (Paquette and Helz, 1995), polysulfides (Paquette and Helz, 1997; Jay et al., 2000), and humic substances (Ravichandran et al., 1998, 1999; Waples et al., 2005). In the presence of Fe(III)-(hydr)oxides, S(-II) is rapidly oxidized, with the dominant product being elemental sulfur [S(0)] (Pyzik and Sommer, 1981; Poulton et al., 2004):

$$2\mathrm{FeOOH} + \mathrm{HS}^- + \mathrm{H_2O} \rightarrow \mathrm{S(0)} + 2\mathrm{FeOH}^+ + 3\mathrm{OH}^-. \quad (3)$$

In addition to Fe(III), S(-II) may react with S(0) to form polysulfide (S_x^{2-}) at neutral to basic pH, providing a potential mechanism for $HgS_{(s)}$ dissolution:

$$\mathrm{HgS_{(s)}} + \mathrm{HS}^- + 2(x-1)\mathrm{S(0)} \rightarrow \mathrm{Hg(S_x)_2}^{2-}{}_{(aq)} + \mathrm{H}^+ \quad (4)$$

$$\mathrm{HgS_{(s)}} + (x-1)\mathrm{S(0)} + \mathrm{H_2O} \rightarrow \mathrm{HgS_xOH}^-{}_{(aq)} + \mathrm{H}^+ \quad (5)$$

at low (10^{-5}–10^{-4} M) sulfide concentrations (Jay et al., 2000) and

$$\mathrm{HgS_{(s)}} + \mathrm{HS}^- + (x-1)\mathrm{S(0)} \rightarrow \mathrm{Hg(S_x)(SH)}^-{}_{(aq)} \quad (6)$$

at higher (10^{-3}–10^{-2} M) sulfide concentrations (Paquette and Helz, 1997). Whether iron reacts with $HgS_{(s)}$ under anaerobic conditions is currently unknown. Fe(II) adsorbs to Fe(III)-(hydr)oxides and may compete for surface sites with Hg(II) (Charlet et al., 2002). Fe(II) is also a reductant, and its oxidation could conceivably couple to Hg(II) reduction. The reactivity—specifically the reductive potential—of Fe(II) formed via reductive dissolution of Fe(III)-(hydr)oxides by S(-II) is a critical unknown when evaluating the possibility of Hg(II) reduction as a mode of Hg release. While aqueous Hg(0) can volatilize, some fraction is believed to reoxidize to form reactive Hg(II) (Fitzgerald and Lamborg, 2003). As discussed in Section 5.3, the potential for Fe(II) to react with the most stable form of Hg(II), $HgS_{(s)}$, should also be considered.

The speciation of Fe(II) will determine its reactivity as a reductant (Stumm and Sulzberger, 1992; Silvester et al., 2005) and, therefore, the likelihood that it will reductively dissolve adsorbed or solid Hg(II) in nature. Once bound to an Fe(III)-bearing mineral surface, sulfide may reduce up to two neighboring ferric ions, forming Fe(II) and oxidized sulfur species, of which elemental sulfur is likely most stable (Pyzik and Sommer, 1981; dos Santos Afonso and Stumm, 1992; Poulton et al., 2004). Although Fe(II) is more labile than Fe(III), its dissolution is usually slow

(dos Santos Afonso and Stumm, 1992). Fe(II) has been found to transform Fe(III)-(hydr)oxides into mixed-valence, Fe(II)/Fe(III) minerals such as magnetite ($Fe^{II}Fe_2^{III}O_4$) and green rust (e.g., $Fe_4^{II}Fe_2^{III}(OH)_{12}\cdot SO_4\cdot nH_2O$) in both abiotic systems (Taylor and McKenzie, 1980) and systems containing iron-reducing bacteria (Frederickson et al., 1998; Hansel et al., 2004). Fe(II) bound to Fe(III)-(hydr)oxide surfaces has been found to reduce dissolved Hg(II) to Hg(0) (Charlet et al., 2002). Hydroxysulfate green rust has also been found to reduce dissolved Hg(II) to Hg(0) (O'Loughlin et al., 2003). Whether similar species of Fe(II) can react with $HgS_{(s)}$ is currently unknown. The consequences of such reactivity would be significant in assessing the long-term stability of the commonly considered unreactive $HgS_{(s)}$.

2. Materials and methods

2.1. Materials

Goethite was synthesized according to the method of Atkinson et al. (1968), dialyzed, and stored as an aqueous suspension under N_2 at 4 ° C. X-ray diffractograms exhibited characteristic goethite peaks and SEM micrographs exhibited crystals with a nearly uniform, approximately 20 by 200 nm prismatic morphology. In aqueous suspension, photon correlation spectroscopic measurements were consistent with a monodispersion of 250 nm (spherically equivalent) particles. The BET specific surface area (SSA) was determined to be 90 $m^2\ g^{-1}$.

The preparation of batches of Hg(II) adsorbed to goethite suspensions and bisulfide solutions, and the handling of samples taken during sulfidation experiments were performed in a 2% H_2 in N_2 glove bag equipped with Pd catalysts to remove oxygen. Water used for all of these purposes was prepared by heating deionized, 18.2 MΩ cm water to 80 ° C for 30 min, purging with ultra-high purity (<1 ppm O_2) N_2 for 45 min while cooling, and storing in the glove bag for at least 12 h prior to use (hereafter referred to as reagent water).

Bisulfide stock solutions (approx. 25 mM) were prepared using $Na_2S{\cdot}9H_2O$ crystals (Fisher Scientific, lot No. 037616) that had been stored in air at 4 °C and washed in the glove bag with reagent water. Aqueous Hg(II) stock solutions were prepared from a standardized 997 μg mL^{-1} (4.97 mM) solution preserved in 1.2 wt% HNO_3 (Aldrich, lot No. 12523JC). A bromine monochloride solution, used to preserve dissolved Hg samples, was synthesized using Fisher Omni*Trace* conc. HCl, 99.8% potassium bromate (Sigma–Aldrich), and 99+% potassium bromide (Aldrich). Reagent-grade *N*,*N*-dimethyl-*p*-phenylenediamine sulfate (Sigma), ferrozine ($C_{20}H_{13}N_4S_2O_6Na{-}H_2O$; Acros Organics 98+%), and HEPES buffer were used to make colorimetric reagents. Standardized solutions of sodium thiosulfate (Fisher, lot No. 035854-24) and iodine (Aldrich, lot No. 05106EU) were used to standardize S(-II) stock solutions. Standardized solutions of 0.1 M NaOH and HNO_3 were used to adjust pH.

2.2. Stirred-flow reactor (sulfidation) experiments

Prior to starting the sulfidation experiments, in the glove bag, Hg(II) [mostly $Hg(OH)_2$, based on the pH and composition of the system (Hepler and Olofsson, 1975)] was sorbed to a 5 g L^{-1} batch suspension of goethite. To avoid strong chemical microenvironments, the Hg stock solution (4.97 mM in 1.2% HNO_3) was prediluted to 125 or 350 μM (according to the Hg concentration desired for the experiment) in approximately 100 mL and adjusted to pH 3 with NaOH prior to mixing with pH 5.5 goethite suspension in pyrex bottles. While vigorously stirring, several mL of prediluted Hg solution was added to the goethite suspension, alternately adding drops of 0.1 or 1 M NaOH, eventually reaching pH 7.5 ± 0.1 and a 250 ± 5 mL total volume. Total Hg concentrations ranged from 20 to 180 μM. The estimated ionic strength of the suspensions was 10 mM based on the reagents added during preparation. The bottles were agitated for one to two days.

Bisulfide solutions (approximately 0.5 or 1 mM) were prepared by diluting stock solution to 500 or 1000 mL in volumetric flasks with oxygen-free water. To lessen chemical microgradients during sulfidation of goethite, the pH of bisulfide solutions was adjusted from 12 to approximately 9. The S(-II) concentrations of these solutions were determined both iodimetrically and colorimetrically (Section 2.3.2). The solutions were sealed in Pyrex bottles equipped with a bag that allowed N_2:H_2, 98:2 gas to backfill as bisulfide was pumped out.

A 1-L glass reaction vessel fitted with several inlet and outlet ports (Fig. EA1, electronic annex) served as the reactor for all experiments. Plastic components were secured to the reactor via fritted glass fittings. Glass tubing, mounted using nylon and viton o-ring compression fittings, ensured precise placement of tubing during the course of experiments. PEEK tubing was used to deliver bisulfide solution using a piston (HPLC) pump at 1 mL min^{-1}.

To start the sulfidation experiment, the Hg-goethite suspension was poured into the reactor while sparging with N_2. Magnetic stirring commenced with continued N_2 sparging for 20–30 min. An initial sample was then taken prior to starting the sulfide pump, with periodic sampling thereafter.

The pH of the reactor suspension was continually monitored and maintained at 7.5 ± 0.2 by a Radiometer Titralab 856 titration system equipped with a sulfide-resistant double-junction pH electrode and two 10 mL burettes containing 100 mM HNO_3 and 50 mM NaOH that had been bubbled with N_2.

Periodic sampling was performed by extracting 20–35 mL of suspension through Teflon tubing from the reactor into a 50-mL glass syringe. The syringe was sealed using a stopcock and then transferred into the glove bag. Solids were mounted on 0.2 μm polyethersulfone (PES)

membranes supported by polypropylene cartridges for chemical and spectroscopic measurements, while aliquots of filtrate were retained for analysis of dissolved (i.e., <0.2 μm) constituents (Section 2.3). Used syringes and filter cartridges were rinsed and sonicated in detergent (removing residual particles); soaked in a 0.5% BrCl solution (removing residual Hg); rinsed with deionized water, soaked in 1 M HNO_3, and rinsed again with deionized water (to remove residual chloride from the BrCl rinse). Carryover of Hg was negligible based on analysis of several filter blanks. In all, the results of six sulfidation experiments are presented in this paper (Table 1).

2.3. Aqueous constituent analyses

In the following sections, dissolved constituents are defined as those capable of passing 0.2 μm PES filters.

2.3.1. Dissolved mercury

Filtered samples to be analyzed for Hg were oxidized at room temperature by adding a bromine monochloride-hydrochloric acid solution to 0.5 mM BrCl plus 60 mM HCl in glass vials with Teflon-lined caps, diluted, then analyzed using 0.13 M $SnCl_2$ plus 0.12 M HCl reduction, purge and trap dual gold amalgamation, and cold vapor atomic fluorescence spectrometry (CVAFS), based on U.S. Environmental Protection Agency method 1631. In a class 1000 clean lab, using an analytical balance, samples were diluted in polypropylene tubes to 10–100 ng Hg L^{-1} (3σ of triplicate blank recoveries ranged from 1 to 2.7 ng L^{-1}) with 40 mL of 1 v/v% conc. HCl and analyzed within an hour. This level of acidity was required to prevent retention of Hg on polypropylene tube walls, based on our own tests and previous studies (Parker and Bloom, 2005). Five-point fluorescence peak area calibration curves were derived from analysis of standard solutions containing 1–100 ng-Hg L^{-1} prepared from an independently standardized 1 μg L^{-1} stock solution that was stored in a Teflon FEP bottle at 4 ° C in the dark.

CVAFS system checks and cleaning were performed after every 5–8 sample analyses, including: removal of any significant Hg accumulation on the gold traps by heating and purging with argon followed by successive analysis of deionized water and a 10–100 ng L^{-1} standard solution. If more than 2 ng-Hg L^{-1} was recovered from deionized water, residual Hg was removed by running a 5% v/v aqua regia (10:7, HCl:HNO_3) solution through the CVAFS system. Analytical precision was limited by sample dilutions prior to analysis, with replicate relative differences (including sample preparation and instrumental variance) ranging from 5% to 14% of the dilution-corrected Hg concentration (i.e., that in the original sample).

2.3.2. Dissolved sulfide and ferrous iron

Sulfide stock and reactor influent solutions were iodimetrically standardized in triplicate (Clesceri et al., 1998). Based on tests, quantitative recovery required titration of at least half the iodine equivalents in the test solution by the S(-II) in the sample. Dissolved S(-II) in samples taken during sulfidation experiments was measured colorimetrically (Cline, 1969), with a detection limit of 0.5 μM (3σ of reagent blank recoveries) and precision of $1\sigma = 0.6$ μM at the 5 μM concentration level (12%). Dissolved Fe(II) was colorimetrically determined by measuring at 562 nm a solution containing 1 mL of sample and 0.1 mL of ferrozine reagent (1 g L^{-1} ferrozine plus 50 mM HEPES), with a detection limit of 0.02 μM (3σ of reagent blank recoveries) and precision of $1\sigma = 0.1$ μM at the 5 μM concentration level (2%).

2.3.3. Solid-phase ferrous iron

In the glove bag, 10–20 mg of dried solids obtained during sulfidation experiments were ground with an agate mortar and pestle, transferred to a glass vial, weighed, and mixed in the dark with approximately 20 mL of 0.5 N HCl. After 1 week, the suspension was filtered through a 0.2 μm PES membrane, diluted with reagent water, and split into two 1 mL aliquots. One aliquot was mixed with 0.1 mL of 0.4 M hydroxylamine hydrochloride followed by ferrozine (recovering dissolved Fe(III) and Fe(II)) while the other was mixed with ferrozine only (recovering Fe(II)). To ensure favorable pH conditions for Fe(II)-ferrozine complexation (Stookey, 1970), both aliquots were mixed with 0.1–0.2 mL of 5 M ammonium acetate buffer after adding ferrozine. Absorbances of these mixtures were then measured at 562 nm within an hour.

Table 1
Parameters of the sulfidation experiments

Experiment	Sulfide flux (μM h^{-1})	Sulfidation rate[a] (μM h^{-1} m^{-2})	Total Hg (μM)	Initial Γ (nmol Hg m^{-2})	Maximum sulfide loading[b]	Figure cross reference
(a)	210	1.9	20	30	2.9	Figs. 2, 5, 9 and 10
(b)	250	2.2	100	90	3.0	Figs. 3 and 8
(c)	50	0.5 ± 0.2	15	35	0.20	Fig. 4
(d)	40	0.4	20	35	0.14	Fig. 4
(e)	80	0.7 ± 0.1	180	180	0.20	Figs. 6, 7a; Table 2
(f)	310	2.8 ± 0.3	180	180	0.60	Fig. 7b

[a] Calculated from sulfide flux and the initial Fe concentration in the reactor (e.g., Fig. 1). Errors were derived from uncertainty in the concentration of sulfide in the influent solutions. Where no errors are indicated, uncertainty is in accordance with the significant digits reported.
[b] Units are μmol S(-II) μmol^{-1} ≡FeOH, or dimensionless (see Section 3).

2.3.4. EXAFS and XANES spectroscopy

Solids retained on filter membranes were dried at room temperature in the glove bag, sealed with Kapton tape, and stored under N_2 prior to analysis. Hg L_{III} and Fe K-edge EXAFS spectra were measured at room temperature on wiggler-magnet Molecular Environmental Sciences Beamline 11-2 at the Stanford Synchrotron Radiation Laboratory (SSRL) and bending magnet beamline 13-BM-D of the GeoSoilEnviro Consortium for Advanced Radiation Sources at the Advanced Photon Source (APS) using cryogenically cooled Si(220) (SSRL) or Si(111) (APS) double-crystal monochromators. Fluorescence-yield data were collected with Canberra 30-element (SSRL) and 16-element (APS) solid-state (Ge) detectors. Harmonic rejection mirrors were used to allow full tuning of monochromators during Hg EXAFS measurements. During Fe EXAFS measurements, however, the monochromators were detuned by approximately 50%.

Sulfur K-edge X-ray absorption near edge structure (XANES) spectra were collected on wiggler beamline 6–2 at SSRL, which is equipped with a single-channel fluorescence detector and a Ni-coated harmonic rejection mirror, allowing full tuning of the Si(111) double crystal monochromator. The X-ray flight path and sample chamber were purged with helium gas. In the glove bag, solids were mounted on Kapton tape and covered with a thin polycarbonate film and transported to the beamline in a sealed box containing N_2. Calibration energies defined by the first maximum of the first derivative of absorption edges of sodium thiosulfate (2472 eV) and elemental sulfur (2471.5 eV) were periodically monitored. Other reference compounds analyzed included potassium sulfite and sodium sulfate. The X-ray absorption edges of sample spectra were compared to those of the reference compounds to determine the sulfur oxidation states present.

Quantitative speciation of Hg in the sulfidized goethite solids was performed by heuristic analysis of Fourier-transformed, k^3-weighted Hg L_{III} EXAFS, or radial structure functions (RSF). RSFs contain peaks corresponding to pair correlations between X-ray absorbing Hg atoms and backscattering, nearest-neighbor oxygen and sulfur atoms (Brown et al., 1988). The amplitude of each respective pair correlation (i.e., the moduli of Fourier-transformed, k^3-weighted EXAFS, $\overline{F}$) is assumed to quantitatively comprise Hg–oxygen and Hg–sulfur pair correlations, exclusively representing Hg(II) adsorbed on goethite and metacinnabar (β-$HgS_{(s)}$), respectively. These pair correlations were modeled according to phase-shift and amplitude functions calculated using the *ab initio* code FEFF 7 (Zabinsky et al., 1995) for the HgO (montroydite) structure, a plausible goethite surface complex model (Tiffreau et al., 1995; Kim et al., 2004b), and Hg bound to sulfur in the β-$HgS_{(s)}$ cubic mineral structure. To obtain mass fractions of Hg adsorbed on goethite and β-$HgS_{(s)}$, $\overline{F}$ is deconstructed as the sum of each species' coordination number, *CN*, multiplied by its mass fraction, *f*, according to the following proportionality:

$$\overline{\mathrm{F}}(k^3 \cdot \chi(k)) \propto f_{\mathrm{adsorbed}} CN_{\mathrm{Hg-O}} + (1 - f_{\mathrm{adsorbed}}) CN_{\mathrm{Hg-S}} \quad (7)$$

Average Hg–O and Hg–S interatomic distances were constrained by fitting each pair correlation individually according to a least-squares minimization using IFEFFIT (Newville, 2001) via the Sixpack interface (Webb, 2005). Initial approximations of coordination numbers (*CN*) were obtained from these preliminary fits. Initial values for the Debye–Waller factors (σ^2) for the Hg–O and Hg–Fe frequencies of the adsorbed Hg species were obtained by fitting an EXAFS spectrum of Hg adsorbed to goethite in the absence of sulfide, guided by previous work (Kim et al., 2004b). Because of the structural (and potential thermal) disorder characteristic of heavy metal adsorption complexes, refinement of σ^2 for the Hg–Fe frequencies was not feasible to a statistically significant extent. A value of $\sigma^2 = 0.01$ Å^2 was henceforth used without further adjustment. Similarly, σ^2 for the Hg–S frequency was based on fitting an EXAFS spectrum of pure β-$HgS_{(s)}$. σ^2 values for the Hg–O and Hg–S frequencies (Hg–Fe frequencies were not detectable in the sulfide-amended samples) were refined in fits of the sulfide-amended sample EXAFS spectra according to their augmented reduction of EXAFS amplitude at higher *k* compared to coordination number (Teo, 1986). Amplitude reduction factors (S_0^2) were constrained based an approach presented by Ravel (2000): S_0^2 values of 0.83 and 0.9 for the Hg–O and Hg–S pair correlations, respectively, were used. While constraining the *CN* of the adsorbed and HgS species, f_{adsorbed} was allowed to float during simultaneous fitting of both pair correlations. Fitting of overlapping RSF peaks were constrained according to sulfidation experiment systematics. Specifically, as sulfidation progressed, solid samples exhibited less (more) of a Hg–oxygen (sulfur) characteristic peak. Sensitivity analyses of the influence of changes in coordination numbers ($CN \pm 20\%$) and Debye–Waller factors ($\sigma^2 \pm 0.01$ Å^2) on f_{adsorbed} were performed, according to estimates of the inherent errors of these parameters as measured by EXAFS (Brown et al., 1988).

2.4. Thermodynamic modeling

To evaluate the possible existence of dissolved Hg species, select dissolved constituents were thermodynamically modeled. The MINTEQ thermodynamic database (http://www.lwr.kth.se/English/OurSoftware/vminteq) was modified to include aqueous Hg–polysulfide complexes according to chemical reactions provided by Paquette and Helz (1997) and Jay et al. (2000), correcting their conditional log*K* values to $I = 0$ M using a modified form of the "B-dot" equation (Helgeson, 1969). This modified database was used with the modeling software Geochemist's Workbench, version 4. Application of the model and its limitations is discussed in Section 5.3.

3. Characterization of experiments

The stirred-flow reactor sulfidation experiments model, in a simplified form, transformations of a particle-associated Hg phase presumably representative of a significant portion

of Hg in the environment (i.e., adsorbed to a Fe(III)-(hydr)oxide) under sulfate-reducing conditions. In this study, a pump introduces sulfide to the system instead of SRB, and the reactor is more Fe(III)-rich than natural systems. To simplify this study, two naturally important constituents were excluded from the sulfidation experiments: organic carbon and bicarbonate. Both would be present where SRB are active, potentially affecting iron, sulfur, and Hg reactivity. Intercomparison of laboratory experiments and reconciliation of their results to natural systems requires scaling of experimental parameters according to the concentrations of geochemically reactive constituents.

Experimental parameters are scaled according to the goethite specific surface area (SSA) (fixed at 90 $m^2\,g^{-1}$), solids concentration (starting at 5 g L^{-1} and corrected for dilution and sampling), and an assumed reactive surface site density of six sites per nm^{-2} (Cornell and Schwertmann, 2003). These quantities yield an estimated molar concentration of sites, denoted as [≡FeOH], ranging from 4.1 to 4.6 mM at the start of experiments and changing thereafter due to dilution and sampling (Fig. 1). The concentration of bisulfide delivered to the reactor was normalized by the estimated concentration of goethite surface sites, yielding a loading parameter, to be referred to hereafter as [S(-II)]:[≡FeOH] or 'sulfide loading.'

Sulfate reduction rates and Fe(III) content measured in natural sediments can be compared to this study's sulfide fluxes (40–310 μM h^{-1}) normalized by the total surface area of the goethite initially present in the reactor (dimensionally μM $h^{-1}\,m^{-2}$; Table 1). For example, Thamdrup et al. (1994) report sulfate reduction rates for coastal marine sediments ranging from 0.4 to 6 μM h^{-1} and 'reactive' Fe(III) concentrations on the order of 10 mM. Assuming this reactive Fe(III) to comprise $Fe(OH)_3$ with a SSA of $100 \pm 50\ m^2\,g^{-1}$, normalized sulfidation rates would be 5×10^{-3} to 7×10^{-2} μM $h^{-1}\,m^{-2}$, or one to three orders of magnitude less than those employed here (Table 1).

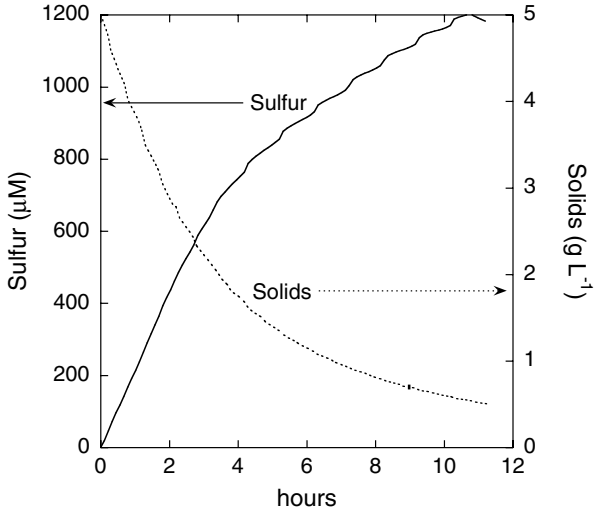

Fig. 1. Change in system composition during sulfidation experiment (b) (Table 1). Ripples in concentrations reflect abrupt volume changes (20–30 mL) due to sampling.

Since the reactivity of sulfide with different Fe(III)-(hydr)oxides varies significantly (Poulton et al., 2004), such comparisons should be considered approximate.

4. Results

4.1. Chemical analyses of aqueous constituents

The dissolved Hg present in an anoxic suspension of goethite rapidly decreases when approximately 2 μM S(-II) $h^{-1}\,m^{-2}$ is added (Figs. 2 and 3). Whether initially at 6.5 or 60 μM, dissolved Hg concentrations decreased to approximately 1 nM by the time the sulfide loading reached 0.05 μmol S(-II) delivered to the reactor μmol^{-1} ≡FeOH, approximately 1 h into the experiment (Figs. 2 and 3). The concentration of sulfur in the reactors rapidly exceeded that of dissolved Hg by a factor of 10 during this period. At a quarter of this sulfidation rate (0.5 μM $m^{-2}h^{-1}$), dissolved Hg concentrations also decreased to 1 nM, but over a 3–7 h experimental period (Fig. 4). Comparing Figs. 2 and 3 with Fig. 4, the rates at which dissolved Hg initially decreases are not significantly different as a function of sulfidation rate. Interestingly, dissolved Hg concentrations eventually began to increase, from 0.2 nM to 10 or 30 nM, at the same point at which dissolved S(-II) and dissolved and solid-phase Fe(II) concentrations became detectable (Figs. 2 and 3).

Dissolved S(-II) was not detected below sulfide loadings of 0.2 μmol S(-II) μmol^{-1} ≡FeOH, whether attained through 2 μM S(-II) $m^{-2}\,h^{-1}$ for 2 h (experiments (a) and (b); Figs. 2 and 3) or through 0.5 μM S(-II) $m^{-2}\,h^{-1}$ for 7 h (experiments (c) and (d)). However, during the 2 μM $m^{-2}\,h^{-1}$ sulfidation experiments, dissolved S(-II)

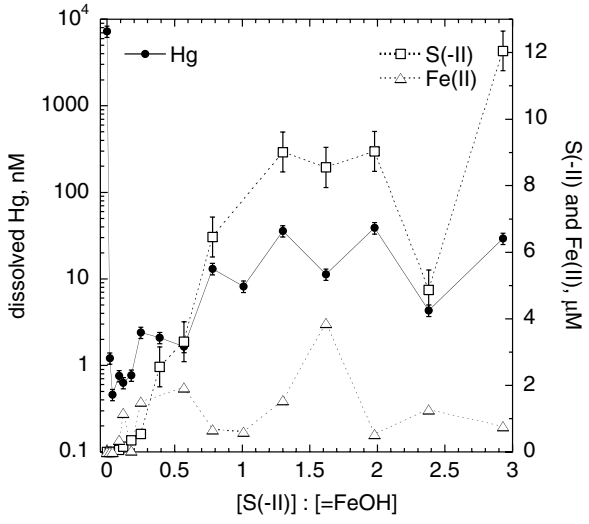

Fig. 2. Dissolved Hg, S(-II), and Fe(II) as a function of sulfide loading during experiment (a): 1.9 μM S(-II) $h^{-1}\,m^{-2}$ applied to 5 g L^{-1} goethite with 30 nmol adsorbed Hg m^{-2} at pH 7.5. Error bars for Hg data represent the maximum variability of replicate sample analyses (approx. 20% of all samples), while those for S(-II) and Fe(II), where visible, are 1 σ of triplicate analyses of a subset of samples (approx. 10%).

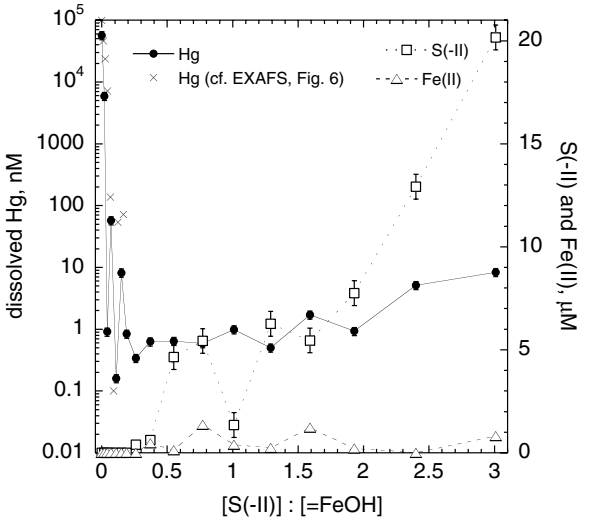

Fig. 3. Dissolved Hg, S(-II), and Fe(II) as a function of sulfide loading during experiment (b) and dissolved Hg for experiment (e) (× symbols; these data accompany EXAFS results for the solid phase presented in Fig. 6): experiment (b) 2.2 μM S(-II) h^{-1} m^{-2} applied to 5 g L^{-1} goethite with 90 nmol adsorbed Hg m^{-2} at pH 7.5. Error bars for Hg data represent the maximum variability of replicate sample analyses (approx. 20% of all samples), while those for S(-II) and Fe(II), where visible, are 1 σ of triplicate analyses of a subset of samples (approx. 10%).

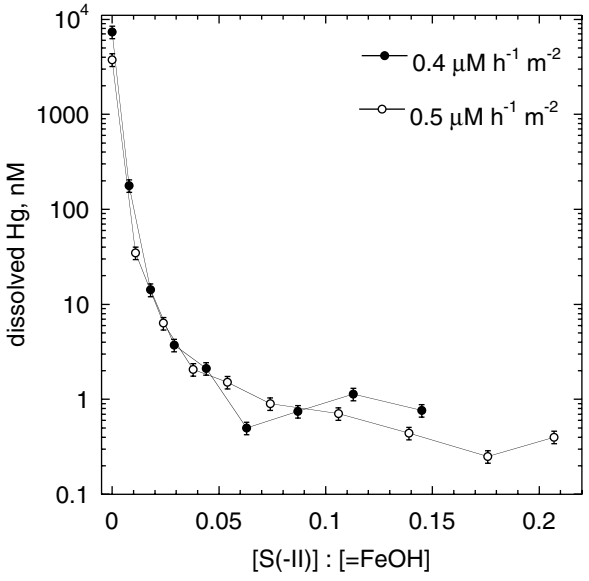

Fig. 4. Changes in dissolved Hg during slower sulfidation rates (experiments c and d) applied to 5 g L^{-1} goethite with 35 nmol adsorbed Hg m^{-2} at pH 7.5. No dissolved S(-II) or Fe(II) were detected during these experiments.

was observed beyond this loading (Figs. 2 and 3). During those periods, concentrations of dissolved S(-II) rose from just above the detection limit (0.5 μM) to plateaus. In the presence of 100 μM total Hg, dissolved S(-II) plateaued at about half the concentration (5 μM; Fig. 3) as in the experiment with 20 μM total Hg (Fig. 2). After these plateaus, dissolved S(-II) concentrations increased again to 12 μM (Fig. 2) or 20 μM (Fig. 3).

Concentrations of Fe(II) in the solid phase steadily increased during sulfidation experiment (a) (Fig. 5), while dissolved Fe(II) fluctuated with no apparent pattern in both experiments (a) and (b). Dissolved Fe(II) concentrations ranged from just above detection (0.02 μM) to 4 μM (Fig. 2) and 1 μM (Fig. 3). During experiment (a), Fe(II) accumulated in the solid phase up to a maximum of 40 μmol g^{-1} before decreasing by about half (Fig. 5). With lower sulfidation rates, dissolved Fe(II) was not detected through sulfide loadings of 0.2 μmol S(-II) μmol^{-1} ≡FeOH (experiments (c) and (d)).

Observations of dissolved Hg, S(-II), and Fe(II) and solid Fe(II) in these experiments provoke speculation as to processes occurring during two distinct periods: the first in which dissolved Hg decreases, and the second in which dissolved Hg increases. An assessment of potential geochemical processes causing these changes, discussed in Section 5, is based on the spectroscopic and microscopic investigations of Hg, Fe, and sulfur speciation reported in the following section.

4.2. Mercury, iron, and sulfur speciation

4.2.1. Mercury speciation

During sulfidation experiment (e), while dissolved Hg concentrations decreased (Fig. 3; × symbols), the concentration of β-$HgS_{(s)}$ increased while that of Hg adsorbed to goethite decreased (Fig. 6). In Fig. 6, the decrease (increase) in the fraction of adsorbed Hg (β-$HgS_{(s)}$) appears as a decrease (increase) in the Hg–O (Hg–S) peak height, according to the model explained in Section 2.3.4. Comparing the EXAFS results of successive pairs of samples in Fig. 6, the fractions of adsorbed Hg decrease and those of HgS increase by 16, 11, and 6 percent through a sulfide

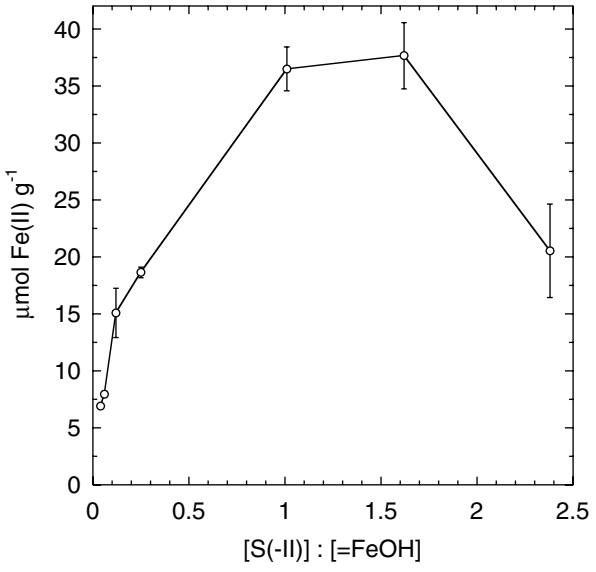

Fig. 5. Concentration of Fe(II) recovered from solids mixed with 0.1 M HCl for 1 week in the dark from sulfidation experiment (a). The error bars reflect the variance of solid masses.

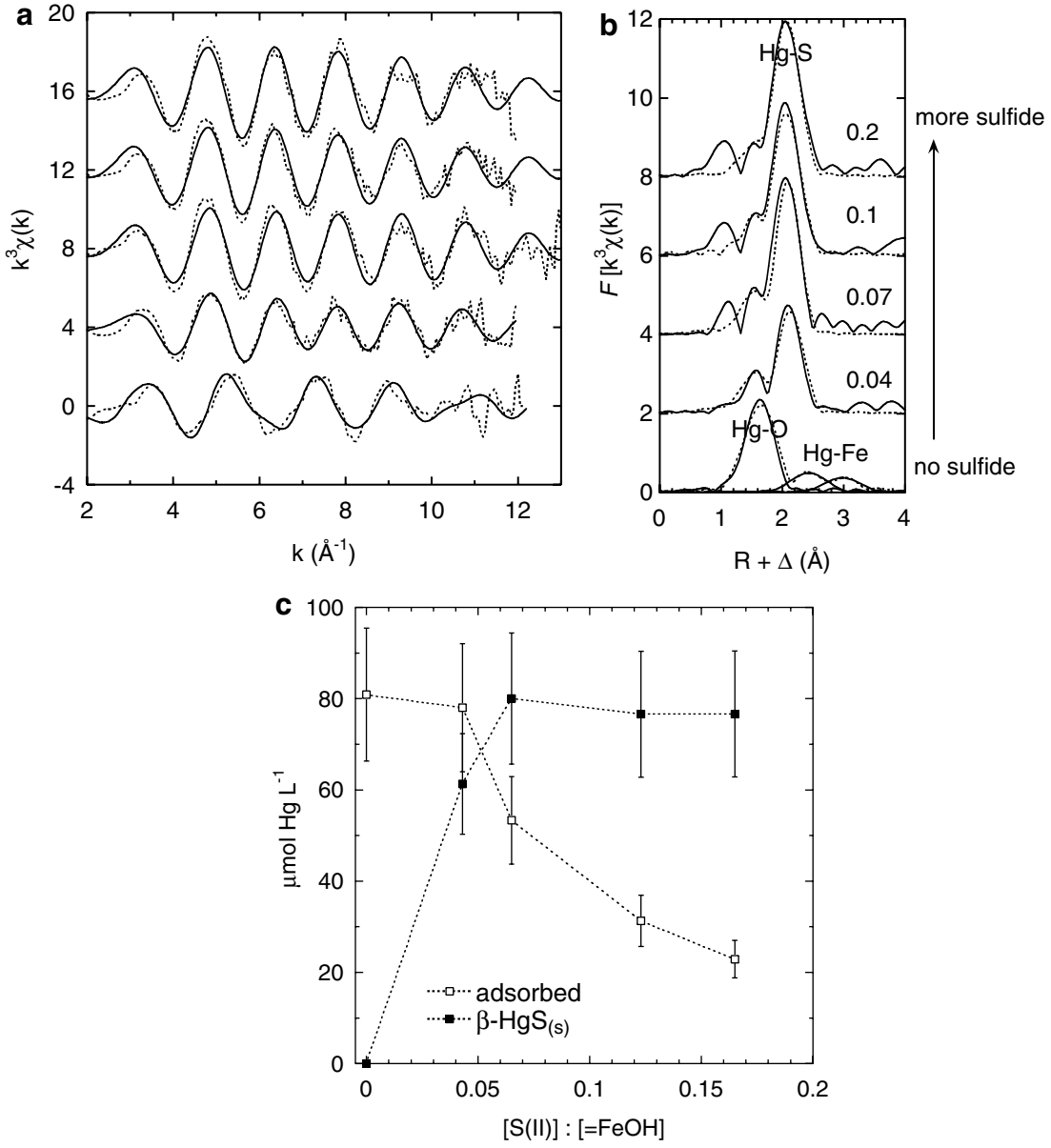

Fig. 6. Hg L_{III}-edge EXAFS (a), radial structure functions (RSF) (b), and quantitative Hg speciation (c) for sulfidation experiment (e). Dotted lines are the experimental data and solid lines are the theoretical fits summarized in Table 2. In (b), Δ is the phase shift of backscattered X-rays and the numbered annotations indicate the sulfide loading at each sample RSF.

loading of 0.2 µmol S(-II) μmol^{-1} ≡FeOH. According to EXAFS measurements of Hg(II) adsorbed to goethite in the absence of sulfide, the apparent Hg–oxygen and Hg–iron coordination numbers and bond distances (Table 2) fit to the experimental data (Fig. 6) do not closely match either a monodentate or bidentate surface complex, but appear to reflect a combination of the two. Coordination numbers fitted to such data are usually rational (i.e., non-integer values) due to bulk averaging of all types of surface complexes present and the error inherent to coordination numbers measured by EXAFS (±20%). As sulfidation progressed during experiment (e), the apparent bulk oxygen coordination number increased (Table 2), suggesting loss of the monodentate Hg, as explained further in Section 5.1. In contrast, adjustment of sulfur coordination numbers did not significantly improve fits to the Hg–S frequency.

While the presence of β-HgS is clearly evident from Hg EXAFS measured from solids sampled throughout sulfidation experiment (c), Hg–oxygen bonding is not evident (data not shown). Approximately 3.2 µmol (630 µg) g^{-1} of Hg in total was used in experiment (c), compared to 16 µmol (3200 µg) g^{-1} total Hg in experiment (e). Detection of adsorbed Hg from these data proved to be impossible, in part because of its low concentration and, more importantly, the presence of the much more structured β-$HgS_{(s)}$.

EXAFS measurements of solids taken during experiment (b) also did not reliably differentiate between adsorbed Hg and $HgS_{(s)}$ species (data not shown). Compared to the previously mentioned systems, this

Table 2
EXAFS results for Hg(II) sorbed to goethite and sulfidation experiment (e)

Loading[a]	R_{Hg-O}		CN_O		σ_O	R_{Hg-Fe}		CN_{Fe}		σ_{Hg-Fe}[b]	R-factor[c]
No sulfide	2.05		2.1		0.006	2.82	3.40	0.7	0.9	0.01	0.130
	Adsorbed phase					$HgS_{(s)}$, metacinnabar					
	f_{ads}	μM_{ads}[d]	R_{Hg-O}	CN_O	σ_{Hg-O}	$f_{\beta\text{-HgS}}$	$\mu M_{\beta\text{-HgS}}$[d]	R_{Hg-S}	CN_{Hg-S}	σ_{Hg-S}	
0	1	81	See above			0	0	—	—	—	—
0.04	0.56	78	2.06	2.3	0.0109	0.44	60	2.53	4.0	0.0070	0.042
0.07	0.40	53	2.05	2.7	0.0080	0.60	80	2.49	4.0	0.0065	0.065
0.1	0.29	31	2.06	3.0	0.0085	0.71	76.60	2.49	4.0	0.0078	0.043
0.2	0.23	23	2.05	3.0	0.0085	0.77	76.64	2.49	4.0	0.0078	0.049

[a] Loading is the molar ratio of sulfide to reactive goethite surface sites ([S(-II)]:[≡FeOH]) as explained in Section 3.
[b] This Debye–Waller factor was fixed for both Hg–Fe EXAFS frequencies based on previous studies (Kim et al., 2004b).
[c] The R-factor is the absolute misfit provided by IFEFFIT: $\sum_{i=1}^{n}\{[\mathrm{Im}(\chi_{dat}(R_i)-\chi_{th}(R_i))]^2+[\mathrm{Re}(\chi_{dat}(R_i)-\chi_{th}(R_i))]^2\}/\{[\mathrm{Im}(\chi_{dat}(R_i))]^2+[\mathrm{Re}(\chi_{dat}(R_i))]^2\}$, where Im and Re are the imaginary and real portions of F and th is the theoretically based fit.
[d] Concentrations of adsorbed Hg and β-HgS were calculated from f_{ads} and the bulk properties of the sulfidation reactor and plotted in Fig. 6c.

system contained an intermediate total Hg concentration: 8.1 μmol (1620 μg) g^{-1}. Oxygen-like frequencies appeared as weak shoulders on the much stronger sulfur frequencies in some RSFs, but not systematically with respect to experimental conditions. While the presence of β-$HgS_{(s)}$ was clearly evident, adsorbed Hg could not be quantified with these EXAFS data. Given the counting rate limitations of current fluorescence detectors used with digital signal processing ('DXP electronics'), reliable differentiation between adsorbed Hg and $HgS_{(s)}$ species in a strongly scattering matrix like goethite using EXAFS spectroscopy appears to require total Hg concentrations in excess of 15 μmol (3000 μg) g^{-1} wherein the fraction of adsorbed Hg is at least 20 percent.

4.2.2. Sulfur speciation

By comparing the X-ray absorption edge energies of samples with those of reference compounds (not shown), sulfur XANES revealed the presence of multiple oxidation states of sulfur in solids sampled during experiment (e), including sulfite [S(IV)] and sulfate [S(VI)] (Fig. 7a). Elemental sulfur [S(0)] was also observed in the XANES spectra of solids sampled after sulfide loadings of 0.04 (Fig. 7a). Similar sulfur oxidation states were observed during a higher sulfidation rate experiment ((f); 2.8 μM h^{-1} m^{-2}; Fig. 7b). No sulfide was detected by XANES during either experiment (e) or (f), the latter of which reached a sulfide loading of 0.6 μmol S(-II) μmol^{-1} ≡FeOH (the highest studied with sulfur XANES), suggesting that the concentration was less than 10 μg g^{-1}. Self-absorption of fluorescent X-rays during XANES measurements was unlikely even for a sample containing the maximum conceivable concentration of sulfur.

4.2.3. Iron speciation

Despite visually observable darkening of goethite suspensions as sulfidation experiment (b) progressed (Fig. EA2, electronic annex), only a small fraction of goethite was transformed by sulfidation. The morphology of most goethite particles observed with SEM after

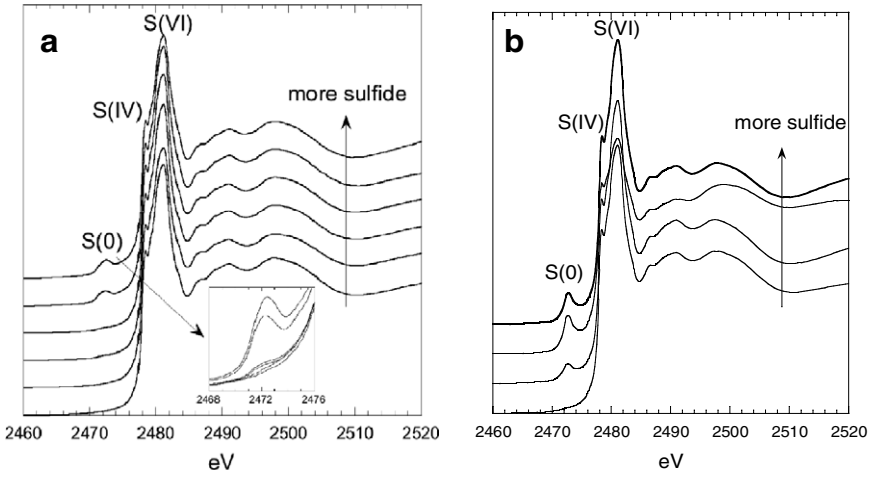

Fig. 7. Normalized sulfur K-edge XANES for solids sampled during (a) sulfidation experiment (e), including sulfide loadings, from bottom to top, of 0.01, 0.03, 0.04, 0.07, 0.10, and 0.20. Spectra are offset for clarity. The inset figure depicts the elemental sulfur region without offsets. (b) Sulfur XANES for experiment (f), including sulfide loadings, from bottom to top, of 0.07, 0.25, 0.40, and 0.60. Sulfur oxidation states were assigned according to the similarity of the absorption edge energies of reference compounds (not shown).

experiment (b) appeared unchanged. Importantly, however, the presence of solids having a different morphology than goethite and composition including sulfur (Fig. 8) suggests that an Fe-bearing phase other than goethite was present at the end of the experiment. Significant fractions (i.e., >10%) of Fe-bearing solid species other than goethite were not detected using Fe K-edge EXAFS (data not shown).

5. Discussion

The following discussion addresses three main issues: (1) the reactivity of S(-II) with Hg(II) vs. goethite and the stability of adsorbed Hg(II), (2) the extent of reductive dissolution of goethite and mineralization of Fe(II), and (3) the influence of byproducts of Fe(III) reduction by sulfide, specifically Fe(II) and polysulfide, on mercury speciation.

5.1. Reactivity of bisulfide with Hg(II) vs. goethite and the stability of adsorbed Hg(II)

Sulfide preferentially reacts with dissolved Hg(II) and, to a lesser extent, with adsorbed Hg(II) over goethite. S(-II) concentrations delivered to the reactor equaled the initial concentration of dissolved Hg within 3 min for the system containing 6.5 μM total Hg (Fig. 2) and 24 min for the 60 μM total Hg experiment (Fig. 3). In both cases, total S(-II) concentrations were only 1–3 percent of the estimated concentration of goethite surface sites. Rapid decreases in dissolved Hg concentrations and the initial absence of detectable S(-II) (Figs. 2 and 3) suggest that S(-II) preferentially reacted with dissolved Hg. During this initial period, the decrease in the adsorbed Hg fraction during one experiment indicates that undercoordinated surface sites (initially 96 percent; Table 1) did not prevent S(-II) from reacting with adsorbed Hg to form β-$HgS_{(s)}$ (Fig. 6).

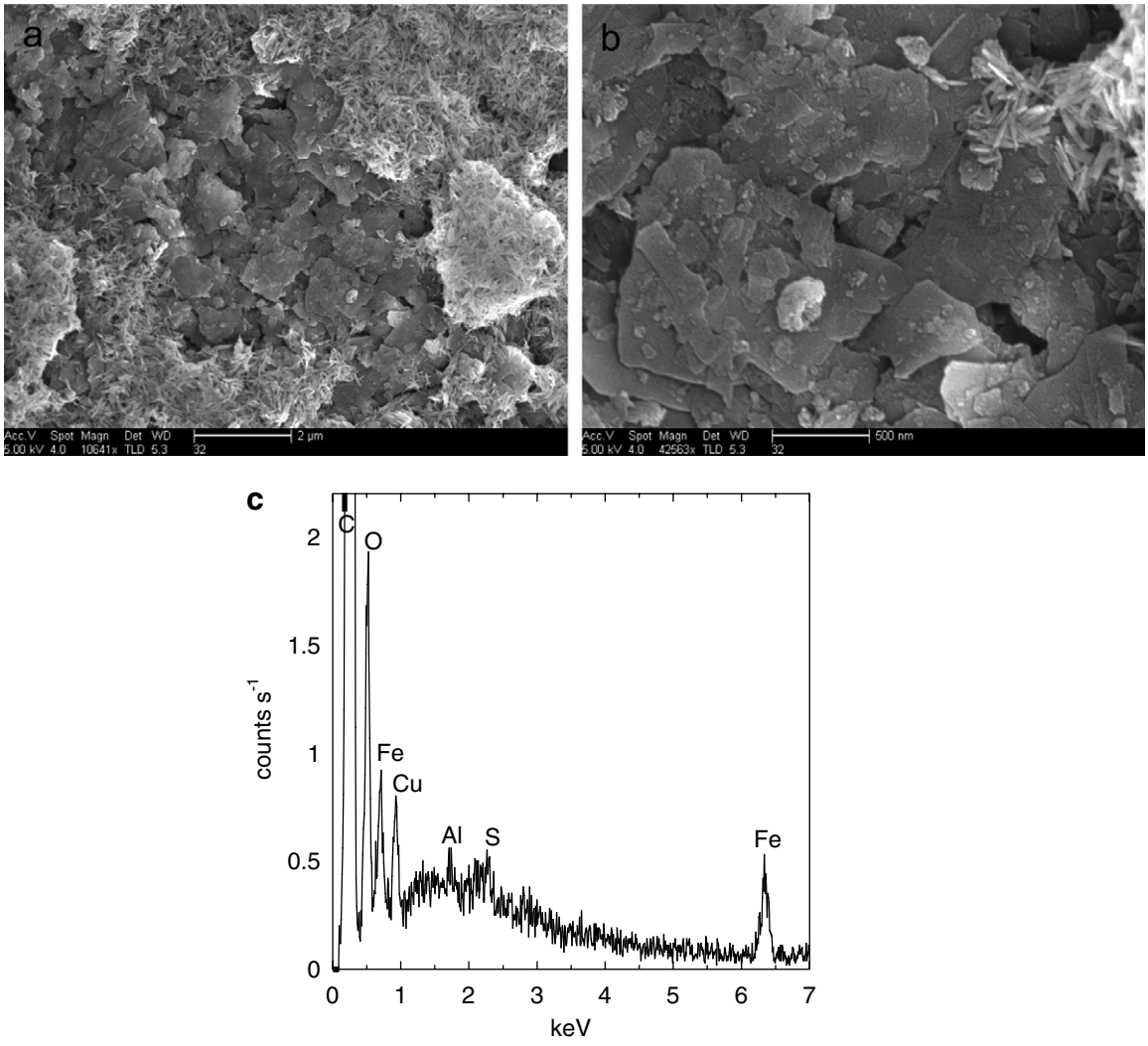

Fig. 8. SEM micrographs of particles taken at the end of sulfidation experiment (b) and shaken in batch at room temperature for 24 h. (a) clustered secondary Fe phase in a goethite matrix (scale bar = 2 μm), (b) closeup of micrograph (a), illustrating poorly formed hexagonal and platy morphology characteristic of sulfate green rust (scale bar = 500 nm), and (c) EDS of 1 μm diameter area of green rust-like particles. Carbon, copper, and aluminum peaks in the EDS arose from the carbon-coated copper grid and aluminum base on which the particles were mounted.

A portion of adsorbed Hg persists through sulfide loadings of at least 0.2 μmol S(-II) μmol^{-1} ≡FeOH. Difficulty in observing the characteristic Hg–oxygen EXAFS frequency in the presence of increasing amounts of β-$HgS_{(s)}$ precluded quantification of adsorbed Hg beyond this loading. As summarized in Table 2, according to EXAFS fits, the coordination number of adsorbed Hg (CN_O) increased from 2.3 to 3.0 as sulfidation progressed. If Hg maintains a solution-oriented oxygen (Tiffreau et al., 1995), a monodentate surface complex would involve two oxygens around Hg while a bidentate surface complex would involve three. Assuming these models are correct, the increase in CN_O fitted to the EXAFS data suggests that monodentate-coordinated Hg is more reactive with S(-II) and that bidentate-coordinated Hg is less reactive. While bidentate Hg-goethite surface complexes have been spectroscopically identified at pH 7.4 (Kim et al., 2004b) and in the presence of sulfate at pH 6 (Kim et al., 2004a), monodentate Hg(II) adsorption complexes on goethite have been postulated using surface complexation models (Gunneriusson and Sjoberg, 1993; Tiffreau et al., 1995; Bonnissel-Gissinger et al., 1999). Further spectroscopic investigation would be required to support the existence of monodentate coordination of Hg on goethite in the presence of various sulfur anions. As dissolved and adsorbed Hg concentrations diminished, S(-II) began to react more extensively with goethite.

5.2. Extent of reductive dissolution of goethite and mineralization of Fe(II)

S(-II) reductively dissolved and partially remineralized goethite, forming a single secondary Fe(II)-bearing phase. This conclusion is based on the loss of S(-II) upon introduction to the reactor, oxidation of S(-II), appearance of solid and dissolved Fe(II), and microscopic observations revealing the secondary phase. Dissolved S(-II) was not detected below sulfide loadings of 0.2 μmol S(-II) μmol^{-1} ≡FeOH (Figs. 2 and 3), regardless of sulfidation rates and time (2 vs. 0.5 $\mu M\ h^{-1}\ m^{-2}$ over 2–7.5 h). Thereafter, less than one percent of the total sulfur delivered to the reactors was recovered as dissolved S(-II) (cf. Figs. 1 and 3). Since S(-II) quickly reached concentrations in excess of Hg in all experiments, reaction with goethite is the primary process by which S(-II) could have initially been removed from solution. The manner in which S(-II) was oxidized is consistent with the reduction of Fe(III)-oxyhydroxide.

Sulfur XANES spectra indicate almost immediate oxidation of S(-II) at the beginning of the sulfidation experiments (Fig. 7), forming S(VI), S(IV), and S(0), all of which have been proposed as products of the reductive dissolution of Fe(III)-(hydr)oxides by S(-II) (Pyzik and Sommer, 1981; dos Santos Afonso and Stumm, 1992; Herszage and dos Santos Afonso, 2000; Poulton et al., 2004). S(0) appears to be the most stable S(-II) oxidation product, as its normalized peak intensity ratios to both sulfite and sulfate increased after sulfide loadings of 0.1 (Fig. 7a) through 0.6 μmol S(-II) μmol^{-1} ≡FeOH (Fig. 7b).

Solid Fe(II)-bearing phases (Fig. 5) could only have originated from Fe(III) reduction at the goethite surface by reaction with S(-II). Dissolved Fe(II) concentrations were at most an order of magnitude less than Fe(II) recovered from solids (Figs. 2, 3, and 5), indicating strong Fe(II) retention. The presence of S(0) (Fig. 7 caption) prior to detection of dissolved Fe(II) (Figs. 2 and 3) also suggests that Fe(II) was initially retained at the goethite surface during reductive transformation by S(-II). Per increment of sulfur added to the reactor (Fig. 1), the incremental amount of Fe(II) formed by the reduction of Fe(III) declined (Figs. 5 and 9), suggesting that the efficiency of reductive dissolution of goethite by S(-II) declined with time. This efficiency was likely controlled by the crystallinity and SSA of goethite and competing reactants such as S(0), resulting in less than approximately 0.5 mol-percent remineralization (based on the highest solid Fe(II) recovery). The rate at which Fe(III) was reduced during experiment (a) is estimated to be on the order of 1 $\mu M\ h^{-1}$, which is within the range reported for marine sediments: 10^{-2}–10 $\mu M\ h^{-1}$ (Thamdrup and Canfield, 2000; Jensen et al., 2003).

The presence of particles having a distinct morphology and size relative to those normally associated with goethite indicate that a secondary Fe-bearing phase formed. The platy and poorly formed hexagonal morphology and sulfur-bearing composition of these particles (Fig. 8), presence of sulfate (Fig. 7), absence of carbonate or chloride (due to

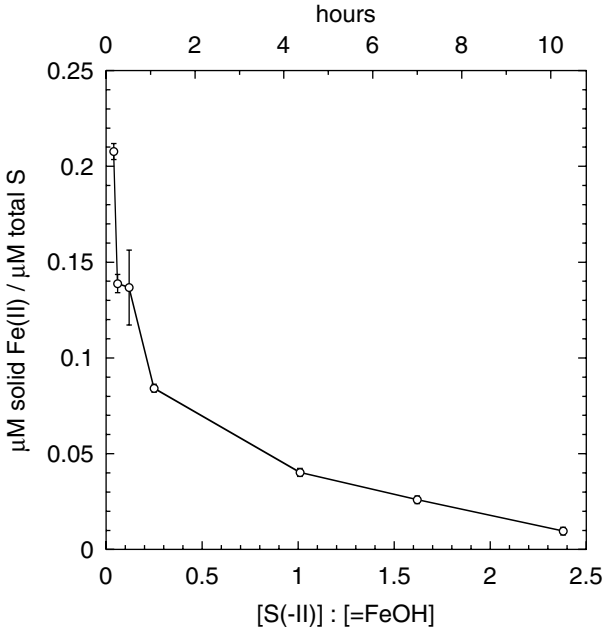

Fig. 9. The concentration of Fe(II) recovered from solids sampled during sulfidation experiment (a) normalized by the total sulfur present in the reactor. Errors bars, some of which are smaller than symbols, reflect error in solid-phase Fe(II) concentrations.

experimental controls), and pH 7.5 are consistent with a poorly formed hydroxysulfate green rust (Genin et al., 1998). How bisulfide oxidation products, surface-bound Fe(II), and mineralized Fe(II) influenced Hg speciation is discussed in the following section.

5.3. Influence of byproducts of Fe(III) reduction by sulfide on mercury speciation

Under the conditions of these experiments, S(0) formed by the oxidation of S(-II) by Fe(III) may have reacted with S(-II) to form polysulfide (S_x^{2-}) that then dissolved adsorbed Hg(II) or β-$HgS_{(s)}$, forming mercury–polysulfide complexes (e.g., $Hg(S_x)_2^{2-}$ (Jay et al., 2000)). In addition, surface-bound Fe(II) may have displaced Hg(II) from goethite, increasing dissolved Hg(II) concentrations (Figs. 2 and 3). S(-II) initially reduced the concentration of dissolved Hg by precipitating β-$HgS_{(s)}$ (Figs. 2–4 and 6). Shortly thereafter, however, dissolved Hg concentrations increased by approximately an order of magnitude (Figs. 2 and 3). Given the dissolved S(-II) present during these periods, Hg(II) was thermodynamically oversaturated with respect to β-HgS (saturation indices $(IAP/K_{sp}) = [S(-II)][Hg(II)]/2 \times 10^{-52}$ (Clever et al., 1985) exceeded 10^{37}).

In experiment (a), rapid increases in both dissolved Hg and solid Fe(II) concentrations coincided (Figs. 2 and 5). For the same experiment, of all constituents measured, the concentration of dissolved Hg correlated with that of solid Fe(II) (Fig. 10). Based on the sulfur XANES results (Fig. 7) and previous studies (Pyzik and Sommer, 1981; Poulton et al., 2004), S(0) is the dominant product of S(-II) oxidation formed during goethite reduction. Accordingly, the observed correlation between dissolved Hg and Fe(II) is more likely a proxy for S(0)-mediated dissolution of Hg. Specifically, polysulfides that were formed once sufficient S(0) and S(-II) were present dissolved β-$HgS_{(s)}$ (Paquette and Helz, 1997; Jay et al., 2000). The apparent tracking of dissolved Hg concentrations with those of S(-II) (which analytically includes polysulfides) during experiment (a) (Fig. 2) is consistent with polysulfide-promoted dissolution of β-$HgS_{(s)}$.

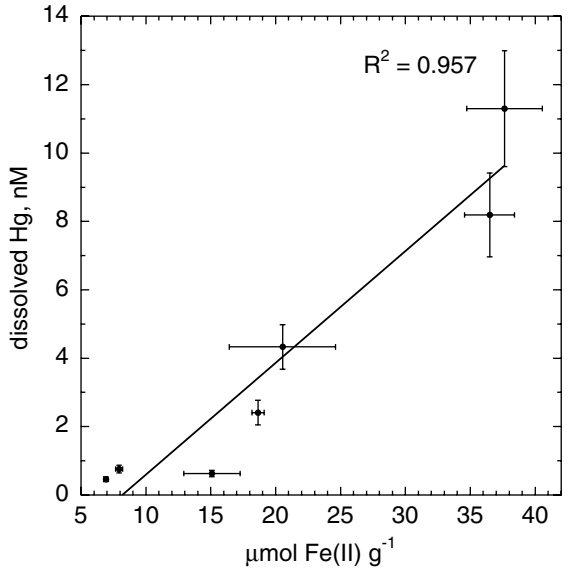

Fig. 10. Apparent correlation between the presence of solid Fe(II)—a proxy for S(0) (see Section 5.3)—and the dissolution of Hg.

To further evaluate the possible formation of dissolved Hg–polysulfide complexes beyond sulfide loadings of 0.2 µmol S(-II) μmol^{-1} ≡FeOH (Figs. 2 and 3), measured S(-II) and estimated concentrations of S(0) were thermodynamically modeled with Geochemist's Workbench (ver. 4), using the MINTEQ database modified to include reaction 4 (Section 1.2.3) (Jay et al., 2000) and/or reaction 6 (Paquette and Helz, 1997). The sulfidation systems were never at equilibrium during experiments. For example, dissolved Hg concentrations decreased by 70–95 percent following storage of suspensions sampled at the end of experiments (a) and (b) under *in situ* conditions for 24 h. Furthermore, the time required to extract samples, filter, and preserve dissolved constituents was likely shorter than the time required for the samples to reach equilibrium. As a result, the reliability of the thermodynamic model depends on whether the samples attained a sufficiently metastable state in which relevant constituents did not change disproportionately. Applying reaction 4 to the sulfidation reactor, the concentration of $HgS_{(s)}$ is well in excess of dissolved Hg concentrations and therefore can be considered to not change during formation of polysulfide complexes. However, S(0) and HS^- are less abundant, and HS^- is reacting with goethite, which suggests that $Hg(S_x)_2^{2-}$ must completely form prior to, but not decompose before, sample preparation in order for the model to mean anything. The tracking of dissolved Hg and S(-II) shown in Fig. 2 suggests that experiment (a) might be characterized as metastable according to these criteria.

In addition to the crucial assumptions above, practical assumptions concerning the concentration of S(0) and system volume were required. According to the stoichiometry of reaction 3, two Fe(III) are reduced per HS^-. Halving the concentrations of solid-phase Fe(II) (Fig. 5), approximately 4–20 µmol S(0) g^{-1} solids is estimated to have formed during experiment (a). Physicochemical reactions with particles, which mostly comprised goethite (Fig. 8), were not included in the model. However, the presence of particles likely co-located adsorbed Hg(II), β-$HgS_{(s)}$, and S(0) by direct adsorption of Hg(II) and as a result of chemical reactions at the surface [i.e., precipitation of β-$HgS_{(s)}$ and HS^- oxidation to S(0)]. The correlation between dissolved Hg and solid Fe(II) and, by proxy, S(0) (Fig. 10) supports surface-mediated reaction mechanisms.

To a first approximation, the relevant concentrations of sorbates in a heterogeneous metastable system are best estimated as their masses divided by an interfacial volume, not the bulk system volume. The interfacial volume was estimated by considering goethite particles as $10 \times 25 \times 250$ nm rectangular prisms with a double layer

thickness (DLT) of 3 nm, based on an ionic strength of 0.01 M (Fig. EA3) [DLT in meters at 25 °C = $\kappa^{-1} = (3.29 \times 10^9\ I^{1/2})^{-1}$; (Stumm and Morgan, 1996)]. Scaling the interfacial volume per particle by the estimated number of goethite particles in a gram, the concentration of S(0) based on solid mass was converted to a concentration based on interfacial volume (detailed calculations are provided in the EA). Based on this exercise, the interfacial concentrations of S(0) ranged from 0.03 to 0.16 M.

For Case (1), Fig. 11 presents the modeled concentration of dissolved Hg species as a function of HS^- activity in a system containing 0.16 M S(0). The model results suggest that an activity of HS^- (a_{HS-}) of 10^{-3}–10^{-2} M would be required to form 1–10 nM $Hg(S_3)_2^{2-}$ comparable to the total dissolved Hg concentrations observed during experiment (a) (Fig. 2). The *bulk* concentration of S(-II) measured during experiment (a) was much less ($a_{HS-} \sim 10^{-5}$; Fig. 2), but the *interfacial* a_{HS-} concentration may have been as high as 10^{-1} M, according to the interfacial volume approximation. For comparison, two additional cases were modeled under the previously modeled conditions, except: Case (2) $a_{S(0)} = 1$; and Case (3) $a_{S(0)} = 0.16$ M and included the species proposed by Paquette and Helz (1997). In Case 2, as expected, the for-

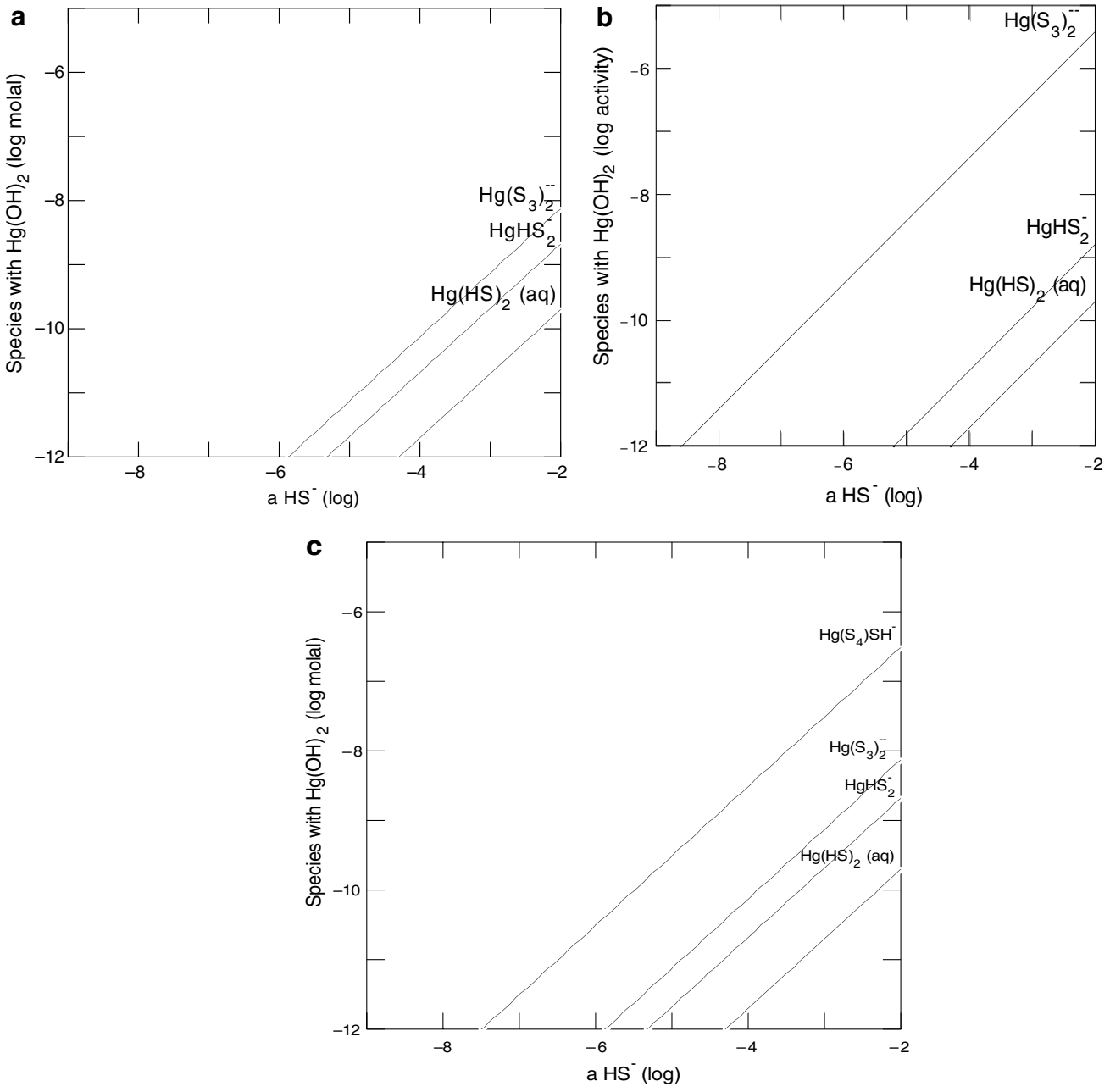

Fig. 11. Thermodynamic model of sulfidation experiment (a). (a) Case 1, according to speciation model proposed by Jay et al. (2000) with $a_{S(0)} = 0.16$, (b) Case 2, same as Case 1, except $a_{S(0)} = 1$, and (c) Case 3, same as Case 1, except species proposed by Paquette and Helz (1997) are included with that proposed by Jay et al. (2000). Mercury-bisulfide complexes were calculated using equations provided in the original MINTEQ database.

mation of $Hg(S_x)_2^{2-}$ is HS^--limited. In Case 3, the concentration of $Hg(S_x)SH^-$ proposed by Paquette and Helz (1997) is more consistent with the total dissolved Hg observed in experiment (a). This result does not provide a basis on which to comment on the relative merits of the Hg–polysulfide models proposed by Jay et al. (2000) versus Paquette and Helz (1997), each of who varied pH and a_{HS-} to develop their models. Clearly, the formation of Hg–polysulfides is also sensitive to $a_{S(0)}$. Future modeling efforts should address this variable in order to comment further on the accuracy of these models. In summary, invoking the assumptions outlined above, the model does not disprove the formation of Hg–polysulfide complexes as a mechanism of β-$HgS_{(s)}$ dissolution in the sulfidation reactors.

Whether adsorbed or mineralized species of Fe(II) directly dissolved Hg is uncertain, although previous studies suggest that either may reduce Hg(II) (Charlet et al., 2002; O'Loughlin et al., 2003). Whether Fe(II) in any form directly dissolved β-$HgS_{(s)}$ cannot be answered by this study. Reduction of Hg(II) in the $HgS_{(s)}$ structure is unlikely, because the sulfide in $HgS_{(s)}$ substantially lowers the redox potential of Hg(II) (Brandon et al., 2001). Considering those experimental conditions most favorable for Hg(II) reduction by adsorbed Fe(II); i.e., pH 7.5 and activities of 10^{-6} HS^- and 10^{-8} $Hg(OH)_2$, the following redox potentials are obtained:

$$HgS + H^+ + 2e^- \leftrightarrow Hg(0) + HS^-$$
$$E_H = -0.35\ V (Brandon\ et\ al.,\ 2001) \quad (8)$$
$$Hg(OH)_2 + 2H^+ + 2e^- \leftrightarrow Hg(0) + 2H_2O$$
$$E_H = +0.36 V (Brandon\ et\ al.,\ 2001) \quad (9)$$
$$\equiv Fe^{III}OFe^{III+} + e^- \leftrightarrow \equiv Fe^{III}OFe^{II+}$$
$$E_H = -0.27 V (Silvester\ et\ al.,\ 2005).^{\dagger} \quad (10)$$

Although somewhat speculative, hydroxysulfate green rust may be able to reduce $HgS_{(s)}$ because it is thermodynamically stable down to an E_H below, for example, −0.35 V at pH 7.5 (Genin et al., 1998). In general, the redox potential of Fe(II) has been observed to span the range of water stability, according to aqueous ligand chemistry (Stumm and Sulzberger, 1992), type of Fe(III) sorbent (Silvester et al., 2005), photochemical effects (Waite and Morel, 1984), and bacteria (Iwahori et al., 2000). Reductive dissolution of HgS by Fe(II) warrants further investigation.

6. Conclusions

Sulfide can directly reduce, but, in the presence of goethite, indirectly enhance the short-term reactivity of Hg, including its potential to be methylated. By reducing Fe(III) in goethite, S(-II) can oxidize to form S(0) and polysulfides that subsequently facilitate the dissolution of $HgS_{(s)}$. Modest amounts of Fe(II) (1–10 μmol g^{-1}) and, by proxy, S(0), formed at rates comparable to those observed in natural sediments (Jensen et al., 2003), and were able to elevate dissolved Hg concentrations by one to two orders of magnitude despite the fact that the continued presence of dissolved S(-II) exceeded nominal β-$HgS_{(s)}$ saturation. The modest fluxes of S(-II) and reactivity of goethite are consistent with the small degree of mineral transformation observed (Poulton et al., 2004). That such small changes significantly affected Hg speciation suggests that interactions between S(-II) and Fe(III) may strongly affect Hg speciation in nature. The extent and timescale by which reductive transformation of Fe(III) by S(-II) enhances Hg reactivity is linked to the abundance and persistence primarily of polysulfide and, perhaps secondarily, Fe(II). This abiotic study provides a useful basis on which to consider biogeochemical processes in systems containing SRB or FeRB.

While prevailing Hg methylation models include dissolved S(-II) as a parameter (Benoit et al., 2003), implicitly accounting for S(-II) sinks such as Fe(III), they fail to consider whether reaction byproducts such as polysulfides and Fe(II) affect Hg reactivity. Recent findings that FeRB can methylate Hg, in some cases to a greater degree than SRB (Fleming et al., 2006), further underscores the need to monitor iron and sulfur in Hg-contaminated natural systems and study interactions of FeRB as well as SRB with Hg under controlled conditions.

Acknowledgments

Experiments performed in this study were funded by an external research grant to AJS from the U.S. Geological Survey Mineral Resources Program and by the U.S. National Science Foundation Environmental Molecular Science Institute at Stanford University (NSF Grant CHE-0431425) (AJS and GEB). XAFS experiments were performed at the Stanford Synchrotron Radiation Laboratory (SSRL) and the Advanced Photon Source, both of which are funded by the Department of Energy's Office of Basic Energy Sciences. SSRL is also supported by the Department of Energy's Office of Biological and Environmental Research, and by the National Institutes of Health. We thank Dr. Mark Marvin-DiPasquale (U.S. Geological Survey) for use of his clean lab and Tekran mercury analyzer. Professor Scott E. Fendorf (Stanford University), Emily J. Fleming (University of California Davis), and two anonymous referees are acknowledged for providing useful comments that improved this manuscript.

Associate editor: David J. Vaughan

[†] E_H is reported for the experimental conditions of the cited work, in which approximately 20-times more adsorbed Fe(II) was present than the maximum total solid Fe(II) observed during sulfidation experiments.

Appendix A. Supplementary data

Supplementary data associated with this article can be found, in the online version, at doi:10.1016/j.gca.2006.11.011.

References

Atkinson, R.J., Posner, A.M., Quirk, J.P., 1968. Crystallization of Fe(III) solutions and hydroxide gels. *J. Inorg. Nucl. Chem.* **30**, 2371.

Bale, A.E., 2000. Modeling aquatic mercury fate in Clear Lake, Calif. *J. Environ. Eng-ASCE* **126**, 153–163.

Barkay, T., Wagner-Dobler, I., 2005. Microbial transformations of mercury: Potentials, challenges, and achievements in controlling mercury toxicity in the environment. In: Laskin, A., Bennett, J., Gadd, G. (Eds.), *Adv. Appl. Microbiol.*, vol. 57. Elsevier Academic Press, San Diego.

Barnett, M.O., Harris, L.A., Turner, R.R., Henson, T.J., Melton, R.E., Stevenson, R.J., 1995. Characterization of mercury species in contaminated floodplain soils. *Water Air Soil Pollut.* **80**, 1105–1108.

Barrow, N.J., Cox, V.C., 1992. The effects of pH and chloride concentration on mercury sorption 1. By goethite. *J. Soil Sci.* **43**, 295–304.

Behra, P., Bonnissel-Gissinger, P., Alnot, M., Revel, R., Ehrhardt, J., 2001. XPS and XAS study of the sorption of Hg(II) onto pyrite. *Langmuir* **17**, 3970–3979.

Benoit, J.M., Gilmour, C.C., Heyes, A., Mason, R.P., Miller, C.L., 2003. Geochemical and biological controls over methylmercury production and degradation in aquatic ecosystems. In: Cai, Y., Braids, O.C. (Eds.), Biogeochemistry of Environmentally Important Trace Elements. 835 ACS Symposium Series Oxford University Press, Oxford.

Benoit, J.M., Gilmour, C.C., Mason, R.P., 2001a. Aspects of bioavailability of mercury for methylation in pure cultures of *Desulfobulbus propionicus* (1pr3). *Appl. Environ. Microbiol.* **67**, 51–58.

Benoit, J.M., Gilmour, C.C., Mason, R.P., 2001b. The Influence of sulfide on solid-phase mercury bioavailability for methylation by pure cultures of *Desulfobulbus propionicus* (1pr3). *Environ. Sci. Technol.* **35**, 127–132.

Benoit, J.M., Gilmour, C.C., Mason, R.P., Heyes, A., 1999. Sulfide controls on mercury speciation and bioavailability to methylating bacteria in sediment pore waters. *Environ. Sci. Technol.* **33**, 951–957.

Bloom, N.S., Moretto, L.M., Scopece, P., Ugo, P., 2004. Seasonal cycling of mercury and monomethyl mercury in the Venice Lagoon (Italy). *Mar. Chem.* **91**, 85–99.

Bonnissel-Gissinger, P., Alnot, M., Lickes, J.P., Ehrhardt, J.J., Behra, P., 1999. Modeling the adsorption of mercury(II) on (hydr)oxides II: alpha-FeOOH (goethite) and amorphous silica. *J. Colloid Interface Sci.* **215**, 313–322.

Brandon, N.P., Francis, P.A., Jeffrey, J., Kelsall, G.H., Yin, Q., 2001. Thermodynamics and electrochemical behaviour of Hg–S–Cl–H_2O systems. *J. Electroanal. Chem.* **497**, 18–32.

Brown Jr., G.E., Calas, G., Waychunas, G.A., Petiau, J., 1988. X-ray absorption spectroscopy and its applications in mineralogy and geochemistry. In: Hawthorne, F.C. (Ed.), *Spectroscopic Methods in Mineralogy and Geology. Rev. Mineral*, vol. 18. Mineralogical Society of America, Washington, DC.

Canfield, D.E., Jorgensen, B.B., Fossing, H., Glud, R., Gundersen, J., Ramsing, N.B., Thamdurp, B., Hansen, J.W., NielsenI, L.P., Hall, P.O.J., 1993. Pathways of organic-carbon oxidation in 3 continental-margin sediments. *Mar. Geol.* **113**, 27–40.

Canfield, D.E., Raiswell, R., Bottrell, S., 1992. The reactivity of sedimentary iron minerals toward sulfide. *Am. J. Sci.* **292**, 659–683.

Charlet, L., Bosbach, D., Peretyashko, T., 2002. Natural attenuation of TCE, As, Hg linked to the heterogeneous oxidation of Fe(II): an AFM study. *Chem. Geol.* **190**, 303–319.

Charnock, J., Moyes, L., Pattrick, R., Mosselmans, J., Vaughan, D., Livens, F., 2003. The structural evolution of mercury sulfide precipitate: an XAS and XRD study. *Am. Mineral.* **88**, 1197–1203.

Clesceri, L.S., Greenberg, A.E., Eaton, A. (Eds.), 1998. *Standard Methods for the Examination of Water and Wastewater*, 20. American Public Health Administration, Washington, DC.

Clever, H.L., Johnson, S.A., Derrick, M.E., 1985. The solubility of mercury and some sparingly soluble mercury salts in water and aqueous-electrolyte solutions. *J. Phys. Chem. Ref. Data* **14**, 631–681.

Cline, I.D., 1969. Spectrophotometric determination of hydrogen sulfide in natural waters. *Limnol. Oceanogr.* **14**, 454–458.

Compeau, G.C., Bartha, R., 1985. Sulfate-reducing bacteria principal methylators of mercury in anoxic estuarine sediments. *Appl. Environ. Microbiol.* **50**, 498–502.

Conaway, C., Watson, E., Flanders, J., Flegal, A., 2003. Mercury deposition in a tidal marsh downstream of the historic New Almaden mining district, California. *J. Phys. IV* **107**, 1421.

Cornell, R.M., Schwertmann, U., 2003. *The Iron Oxides: Structure, Properties, Reactions, Occurrences, and Uses*. Wiley-VCH, Weinheim.

National Research Council, 2000. Toxicological Effects of Methylmercury. National Academies Press, Washington, DC.

dos Santos Afonso, M., Stumm, W., 1992. Reductive dissolution of Iron(III) (Hydr)oxides by hydrogen-sulfide. *Langmuir* **8**, 1671–1675.

Eckley, C.S., Watras, C.J., Hintelmann, H., Morrison, K., Kent, A.D., Regnell, O., 2005. Mercury methylation in the hypolimnetic waters of lakes with and without connection to wetlands in northern Wisconsin. *Can. J. Fish. Aquat. Sci.* **62**, 400–411.

Fitzgerald, W.F., Lamborg, C.H., 2003. Geochemistry of mercury in the environment. In: Lollar, B.S. (Ed.), *Environmental Geochemistry. Treatise on Geochemistry*, 9. Elsevier, St. Louis.

Fleming, E.J., Mack, E.E., Green, P.G., Nelson, D.C., 2006. Mercury methylation from unexpected sources: molybdate-inhibited freshwater sediments and an iron-reducing bacterium. *Appl. Environ. Microbiol.* **72**, 457–464.

Frederickson, J.K., Zachara, J.M., Kennedy, D.W., Dong, H., Onstott, T.C., Hinman, N.W., Li, S., 1998. Biogenic iron mineralization accompanying the dissimilatory reduction of hydrous ferric oxide by a groundwater baterium. *Geochim. Cosmochim. Acta* **62**, 3239–3257.

Gagnon, C., Pelletier, E., Mucci, A., 1997. Behaviour of anthropogenic mercury in coastal marine sediments. *Mar. Chem.* **59**, 159–176.

Genin, J.M.R., Bourrie, G., Trolard, F., Abdelmoula, M., Jaffrezic, A., Refait, P., Maitre, V., Humbert, B., Herbillon, A., 1998. Thermodynamic equilibria in aqueous suspensions of synthetic and natural Fe(II)–Fe(III) green rusts: occurrences of the mineral in hydromorphic soils. *Environ. Sci. Technol.* **32**, 1058–1068.

Gilmour, C., Riedel, G., Ederington, M., Bell, J., Benoit, J., Gill, G., Stordal, M., 1998. Methylmercury concentrations and production rates across a trophic gradient in the northern Everglades. *Biogeochemistry* **40**, 327–345.

Gilmour, C.C., Henry, E.A., Mitchell, R., 1992. Sulfate stimulation of mercury methylation in freshwater sediments. *Environ. Sci. Technol.* **26**, 2281–2287.

Gunneriusson, L., Sjoberg, S., 1993. Surface complexation in the H^+-goethite (alpha-FeOOH)–Hg(II)–chloride system. *J. Colloid Interface Sci.* **156**, 121–128.

Hansel, C.M., Benner, S.G., Nico, P., Fendorf, S., 2004. Structural constraints of ferric (hydr)oxides on dissimilatory iron reduction and the fate of Fe(II). *Geochim. Cosmochim. Acta* **68**, 3217–3229.

Helgeson, H.C., 1969. Thermodynamics of hydrothermal systems at elevated temperatures and pressures. *Am. J. Sci.* **267**, 729–804.

Hepler, L.G., Olofsson, G., 1975. Mercury—Thermodynamic properties, chemical-equilibria, and standard potentials. *Chem. Rev.* **75**, 585–602.

Herszage, J., dos Santos Afonso, M., 2000. The autooxidation of hydrogen sulfide in the presence of hematite. *Colloid Surface A* **168**, 61–69.

Huerta-Diaz, M.A., Morse, J.W., 1992. Pyritization of trace metals in anoxic marine sediments. *Geochim. Cosmochim. Acta* **56**, 2681–2702.

Hunter, J.G., Burger, J., Cooper, K.R., 2003. Use of an integrated mercury food web model for ecological risk assessment. *J. Environ. Sci. Heal. A* **38**, 1201–1214.

Iwahori, K., Takeuchi, F., Kamimura, K., Sugio, T., 2000. Ferrous iron-dependent volatilization of mercury by the plasma membrane of *Thiobacillus ferrooxidans*. *Appl. Environ. Microbiol.* **66**, 3823–3827.

Jay, J.A., Morel, F.M.M., Hemond, H.F., 2000. Mercury speciation in the presence of polysulfides. *Environ. Sci. Technol.* **34**, 2196–2200.

Jay, J.A., Murray, K.J., Gilmour, C.C., Mason, R.P., Morel, F.M.M., Roberts, A.L., Hemond, H.F., 2002. Mercury methylation by Desulfovibrio desulfuricans ND132 in the presence of polysulfides. *Appl. Environ. Microbiol.* **68**, 5741–5745.

Jensen, M.M., Thamdrup, B., Rysgaard, S., Holmer, M., Fossing, H., 2003. Rates and regulation of microbial iron reduction in sediments of the Baltic-North Sea transition. *Biogeochemistry* **65**, 295–317.

Kerin, E.J., Glimour, C.C., Roden, E., Suzuki, M.T., Coates, J.D., Mason, R.P., in press. Mercury methylation by dissimilatory iron-reducing bacteria. *Appl. Environ. Microbiol.* (Available online 20 October 2006).

Kim, C.S., Rytuba, J.J., Brown Jr., G.E., 2004a. EXAFS study of Hg(II) sorption to Fe- and Al-(hydr)oxide surfaces: II. Effects of chloride and sulfate. *J. Colloid Interface Sci.* **270**, 9–20.

Kim, C.S., Rytuba, J.J., Brown Jr., G.E., 2004b. EXAFS study of mercury(II) sorption to Fe- and Al-(hydr)oxides I. Effects of pH. *J. Colloid Interface Sci.* **271**, 1–15.

Kim, C.S., Rytuba, J.J., Brown Jr., G.E., 2004c. Geological and anthropogenic factors influencing mercury speciation in mine wastes: an EXAFS spectroscopy study. *Appl. Geochem.* **19**, 379–393.

King, J.K., Kostka, J.E., Frischer, M.E., Saunders, F.M., 2000. Sulfate-reducing bacteria methylate mercury at variable rates in pure culture and in marine sediments. *Appl. Environ. Microbiol.* **66**, 2430–2437.

King, J.K., Kostka, J.E., Frischer, M.E., Saunders, F.M., Jahnke, R.A., 2001. A quantitative relationship that demonstrates mercury methylation rates in marine sediments are based on the community composition and activity of sulfate-reducing bacteria. *Environ. Sci. Technol.* **35**, 2491–2496.

Lamborg, C.H., Fitzgerald, W.F., O'Donnell, J., Torgersen, T., 2002. A non-steady-state compartmental model of global-scale mercury biogeochemistry with interhemispheric atmospheric gradients. *Geochim. Cosmochim. Acta* **66**, 1105–1118.

Laurier, F., Cossa, D., Breviere, G., Sarazin, G., 2003. Mercury transformations and exchanges in a high turbidity estuary: the role of organic matter and amorphous oxyhydroxides. *Geochim. Cosmochim. Acta* **67**, 3329–3345.

Le Roux, S.M., Turner, A., Millward, G.E., Ebdon, L., Apriou, P., 2001. Partitioning of mercury onto suspended sediments in estuaries. *J. Environ. Monit.* **3**, 37–42.

Lennie, A., Charnock, J., Pattrick, R., 2003. Structure of mercury(II)–sulfur complexes by EXAFS spectroscopic measurements. *Chem. Geol.* **199**, 199–207.

Lowry, G.V., Shaw, S., Kim, C.S., Rytuba, J.J., Brown Jr., G.E., 2004. Particle-facilitated mercury transport from New Idria and Sulphur Bank mercury mine tailings: column experiments and macroscopic, microscopic and spectroscopic analysis. *Environ. Sci. Technol.* **38**, 5101–5111.

Luther, G.I., Church, T.M., 1992. An overview of the environmental chemistry of sulphur in wetland systems. In: Howarth, R.W., Stewart, J.W.B., Ivanov, M.V. (Eds.), *Sulphur Cycling on the Continents*. Wiley, Chichester.

Luther, G.W., Glazer, B., Ma, S.F., Trouwborst, R., Shultz, B.R., Druschel, G., Kraiya, C., 2003. Iron and sulfur chemistry in a stratified lake: evidence for iron-rich sulfide complexes. *Aquat. Geochem.* **9**, 87–110.

Mason, R.R., Abbot, M.L., Bodaly, R.A., Bullock, O.R., Driscoll, C.T., Evers, D., Lindberg, S.E., Murray, M., Swain, E.B., 2005. Monitoring the response to changing mercury deposition. *Environ. Sci. Technol.* **39**, 14A–22A.

Mehrotra, A.S., Horne, A.J., Sedlak, D.L., 2003. Reduction of net mercury methylation by iron in *Desulfobulbus propionicus* (1pr3) cultures: implications for engineered wetlands. *Environ. Sci. Technol.* **37**, 3018–3023.

Mehrotra, A.S., Sedlak, D.L., 2005. Decrease in net mercury methylation rates following iron amendment to anoxic wetland sediment slurries. *Environ. Sci. Technol.* **39**, 2564–2570.

Moye, H.A., Miles, C.J., Phlips, E.J., Sargent, B., Merritt, K.K., 2002. Kinetics and uptake mechanisms for monomethylmercury between freshwater algae and water. *Environ. Sci. Technol.* **36**, 3550–3555.

Newville, M., 2001. IFEFFIT: interactive XAFS analysis and FEFF fitting. *J. Synchrotron Radiat.* **8**, 322–324.

O'Loughlin, E.J., Kelly, S.D., Kemner, K.M., Csencsits, R., Cook, R.E., 2003. Reduction of Ag^{I}, Au^{III}, Cu^{II}, and Hg^{II} by Fe^{II}/Fe^{III} hydroxy-sulfate green rust. *Chemosphere* **53**, 437–446.

Paquette, K., Helz, G.R., 1995. Solubility of cinnabar (red HgS) and implications for mercury speciation in sulfidic waters. *Water Air Soil Pollut.* **80**, 1053–1056.

Paquette, K.E., Helz, G.R., 1997. Inorganic speciation of mercury in sulfidic waters: the importance of zero-valent sulfur. *Environ. Sci. Technol.* **31**, 2148–2153.

Parker, J.L., Bloom, N.S., 2005. Preservation and storage techniques for low-level aqueous mercury speciation. *Sci. Total Environ.* **337**, 253–263.

Poissant, L., Pilote, M., Xu, X., Zhang, H., Beauvais, C., 2004. Atmospheric mercury speciation and deposition in the Bay St. Francois wetlands. *J. Geophys. Res.* **109**, 11.

Poulton, S.W., Krom, M., Raiswell, R., 2004. A revised scheme for the reactivity of iron (oxyhydr)oxide minerals towards dissolved sulfide. *Geochim. Cosmochim. Acta* **68**, 3703–3715.

Pyzik, A., Sommer, S., 1981. Sedimentary iron monosulfides: kinetics and mechanism of formation. *Geochim. Cosmochim. Acta* **45**, 687–698.

Ravel, B., 2000. EXAFS Analysis with FEFF and FEFFIT. Part 2. Commentary. <http://cars9.uchicago.edu/xafs/workshops.html/>.

Ravichandran, M., Aiken, G.R., Reddy, M.M., Ryan, J.N., 1998. Enhanced dissolution of cinnabar (mercuric sulfide) by dissolved organic matter isolated from the Florida Everglades. *Environ. Sci. Technol.* **32**, 3305–3311.

Ravichandran, M., Aiken, G.R., Ryan, J.N., Reddy, M.M., 1999. Inhibition of precipitation and aggregation of metacinnabar (mercuric sulfide) by dissolved organic matter isolated from the Florida Everglades. *Environ. Sci. Technol.* **33**, 1418–1423.

Regnell, O., Ewald, G., Lord, E., 1997. Factors controlling temporal variation in methyl mercury levels in sediment and water in a seasonally stratified lake. *Limnol. Oceanogr.* **42**, 1784–1795.

Regnell, O., Hammar, T., Helgee, A., Troedsson, B., 2001. Effects of anoxia and sulfide on concentrations of total and methyl mercury in sediment and water in two Hg-polluted lakes. *Can. J. Fish. Aquat. Sci.* **58**, 506–517.

Rolfhus, K.R., Lamborg, C.H., Fitzgerald, W.F., Balcom, P.H., 2003. Evidence for enhanced mercury reactivity in response to estuarine mixing. *J. Geophys. Res.* **108**, 3353.

Ryaboshapko, A., Bullock, R., Ebinghaus, R., Ilyin, I., Lohman, K., Munthe, J., Petersen, G., Seigneur, C., Wangberg, I., 2002. Comparison of mercury chemistry models. *Atmos. Environ.* **36**, 3881–3898.

Sakata, M., Marumoto, K., 2005. Wet and dry deposition fluxes of mercury in Japan. *Atmos. Environ.* **39**, 3139–3146.

Silvester, E., Charlet, L., Tournassat, C., Gehin, A., Greneche, J.M., Liger, E., 2005. Redox potential measurements and Mossbauer spectrometry of Fe-II adsorbed onto Fe-III (oxyhydr)oxides. *Geochim. Cosmochim. Acta* **69**, 4801–4815.

Slowey, A.J., Johnson, S.B., Rytuba, J.J., Brown Jr., G.E., 2005a. Role of organic acids in promoting colloid transport of mercury from mine tailings. *Environ. Sci. Technol.* **39**, 7869–7874.

Slowey, A.J., Rytuba, J.J., Brown Jr., G.E., 2005b. Speciation of mercury and mode of transport from placer gold mine tailings. *Environ. Sci. Technol.* **39**, 1547–1554.

Stookey, L.L., 1970. Ferrozine—A new spectrophotometric reagent for iron. *Anal. Chem.* **42**, 779–781.

Stumm, W., Morgan, J.J., 1996. *Aquatic Chemistry. Chemical Equilibria and Rates in Natural Waters*. Wiley-Intersciences, New York.

Stumm, W., Sulzberger, B., 1992. The cycling of iron in natural environments. Considerations based on laboratory studies of heterogeneous redox processes. *Geochim. Cosmochim. Acta* **56**, 3233–3257.

Sveinsdottir, A.Y., Mason, R.P., 2005. Factors controlling mercury and methylmercury concentrations in largemouth bass (*Micropterus salmoides*) and other fish from Maryland reservoirs. *Arch. Environ. Contam. Toxicol.* **49**, 528–545.

Taylor, R.M., McKenzie, R.M., 1980. The influence of aluminum on iron oxides 6. the formation of Fe(II)-Al(III) hydroxy-chlorides, Fe(II)-Al(III) hydroxy sulfates, and Fe(II)-Al(III) hydroxy-carbonates as new members of the pyroaurite group and their significance in soils. *Clays Clay Miner.* **28**, 179–187.

Teo, B., 1986. *EXAFS: Basic Principles and Data Analysis*. Springer.

Thamdrup, B., Canfield, D.E., 2000. Benthic respiration in aquatic sediments. In: Sala, O.E., Jackson, R.B., Mooney, H.A., Howarth, R.W. (Eds.), *Methods in Ecosystem Science*. Springer, New York.

Thamdrup, B., Fossing, H., Jorgensen, B.B., 1994. Manganese, iron, and sulfur cycling in a coastal marine seidment, Aarhus Bay, Denmark. *Geochim. Cosmochim. Acta* **58**, 5115–5129.

Tiffreau, C., Lutzenkirchen, J., Behra, P., 1995. Modeling the adsorption of mercury(II) on (Hydr)oxides 1. Amorphous iron-oxide and alpha-quartz. *J. Colloid Interface Sci.* **172**, 82–93.

Tossell, J.A., 1999. Theoretical studies on the formation of mercury complexes in solution and the dissolution and reactions of cinnabar. *Am. Miner.* **84**, 877–883.

Tossell, J.A., 2001. Calculation of the structures, stabilities, and properties of mercury sulfide species in aqueous solution. *J. Phys. Chem. A* **105**, 935–941.

Tseng, C.M., Amouroux, D., Abril, G., Tessier, A., Etcheber, H., Donard, O.F.X., 2001. Speciation of mercury in a fluid mud profile of a highly turbid macrotidal estuary (Gironde, France). *Environ. Sci. Technol.* **35**, 2627–2633.

Tsui, M.T.K., Wang, W.-X., 2004. Uptake and elimination routes of inorganic mercury and methylmercury in *Daphnia magna*. *Environ. Sci. Technol.* **38**, 808–816.

USEPA, 1997. Mercury Study Report to Congress. EPA-452/R-97-003, <http://www.epa.gov/mercury/report.htm/>.

Waite, T.D., Morel, F.M.M., 1984. Photoreductive dissolution of colloidal iron oxide: effect of citrate. *J. Colloid Interf. Sci.* **102**, 121–137.

Wang, W.X., Wong, R.S.K., 2003. Bioaccumulation kinetics and exposure pathways of inorganic mercury and methylmercury in a marine fish, the sweetlips *Plectorhinchus gibbosus*. *Mar. Ecol. Prog. Ser.* **261**, 257–268.

Waples, J., Nagy, K.L., Aiken, G.R., Ryan, J.N., 2005. Dissolution of cinnabar (HgS) in the presence of natural organic matter. *Geochim. Cosmochim. Acta* **69**, 1575–1588.

Water Science and Technology Board (National Research Council), 2003. Bioavailability of contaminants in Soils and Sediments: Processes, Tools, and Applications. National Academies Press, Washington, DC.

Watras, C.J., Bloom, N.S., Claas, S.A., Morrison, K.A., Gilmour, C.C., Craig, S.R., 1995. Methylmercury production in the anoxic hypolimnion of a dimictic seepage lake. *Water Air Soil Pollut.* **80**, 735–745.

Webb, S.M., 2005. A graphical user interface for XAS analysis using IFEFFIT. *Phys. Scr.* **T115**, 1011–1014.

Whyte, D.C., Kirchner, J.W., 2000. Assessing water quality impacts and cleanup effectiveness in streams dominated by episodic mercury discharges. *Sci. Total Environ.* **260**, 1–9.

Wolfenden, S., Charnock, J.M., Hilton, J., Livens, F.R., Vaughan, D.J., 2005. Sulfide species as a sink for mercury in lake sediments. *Environ. Sci. Technol.* **39**, 6644–6648.

Zabinsky, S.I., Rehr, J.J., Ankudinov, A., Albers, R.C., Eller, M.J., 1995. Multiple scattering calculations of X-ray absorption spectra. *Phys. Rev. B* **52**, 2995.